PENETRATION OF THE SECULAR FIELD THROUGH A MANTLE WITH VARIABLE CONDUCTIVITY

Part I

BY

KEITH LEON McDONALD

TECHNICAL REPORT NO. 19

April 1, 1956

EARTH'S MAGNETISM AND MAGNETOHYDRODYNAMICS

CONTRACT Nonr 1288(00)

OFFICE OF NAVAL RESEARCH

DEPARTMENT OF PHYSICS

UNIVERSITY OF UTAH

SALT LAKE CITY

Penetration of the Secular Field Through A Mantle With Variable Conductivity

Part I

by

Keith Leon McDonald

Department of Physics
University of Utah
Salt Lake City, Utah

Contents

I. Introduction

An extrapolation of the geomagnetic secular variation from the earth's surface to the core-mantle boundary has previously been carried out for an insulating mantle (ref.1). An improved estimate requires a knowledge of the electrical conductivity σ throughout the mantle. This function is roughly known only to about the 700-km depth. With greater depths, it is presumed that σ increases monotonically. The work reported on here is an investigation of the radial distribution of σ.

The work has been divided into two parts. In Part I, we employ a simplified earth model; the core is surrounded by a variably conductive medium of infinite extent. Choosing a power law for σ as function of depth the equations are explicitly integrated in terms of Bessel functions. A surface harmonic expansion at the core, for an arbitrary frequency, is then analytically continued to a distance equal to the earth's radius. Neglecting reflection effects, we thereby obtain the wave attenuation and phase retardation after propagation through the mantle.

Our results show that, after the initial rapid rise in the first 700 or 800 km of the mantle (cf. ref. 2), the conductivity levels off. σ at the 1000 km depth is of the order of 1/10 the value at the core-mantle boundary.

In Part II we consider aperiodic solutions of some relevant models together with the continuations from Part I.

II. Mantle Equations

For later reference, we catalog the quasi-stationary field equations applicable to the Earth's mantle. The general theory of electromagnetic induction in non-uniform conductors has been formulated by Lahiri and Price (1939). The following work draws to some extent on their formalism.

Equating Maxwell's displacement current to zero we obtain the quasi-stationary field equations (in Gaussian units) for a general linear isotropic medium,

$$\nabla \times \underset{\sim}{E} = -\frac{1}{c}\dot{\underset{\sim}{B}} \qquad \nabla \cdot \underset{\sim}{B} = 0 \tag{1}$$

$$\nabla \times \underset{\sim}{H} = \frac{4\pi}{c}\underset{\sim}{J} \qquad \nabla \cdot \underset{\sim}{D} = 4\pi\epsilon \tag{2}$$

The material equations are

$$\underset{\sim}{D} = K\underset{\sim}{E}, \quad \underset{\sim}{B} = \mu\underset{\sim}{H}, \quad \underset{\sim}{J} = \sigma\underset{\sim}{E}.$$

From the first of Eqs. (2), it follows that $\underset{\sim}{J}$ is approximately solenoidal. Neglecting $\dot{\epsilon}$ compared to $\epsilon\sigma/K$, the second of Eqs.(2) gives the approximation

$$4\pi\epsilon = \underset{\sim}{J} \cdot \nabla\left(\frac{K}{\sigma}\right). \tag{3}$$

Thus the space-charge density vanishes only if (a) $\underset{\sim}{J}$ lies in the iso-level surfaces K/σ = constant, or (b) if K/σ is a constant. From (1) and (2), $\underset{\sim}{E}$ and $\underset{\sim}{H}$ must satisfy the equations

$$\nabla \times \left[\frac{1}{\rho}\nabla \times \underset{\sim}{E}\right] + k\sigma\dot{\underset{\sim}{E}} = 0 \tag{4a}$$

$$\nabla \times \left[\frac{1}{\sigma}\nabla \times \underset{\sim}{H}\right] + k\mu\dot{\underset{\sim}{H}} = 0 \tag{4b}$$

where $k = 4\pi/c^2$. On the other hand, in terms of the vector potential $\underset{\sim}{A}$ we have

$$\underset{\sim}{B} = \nabla \times \mu\underset{\sim}{A}, \quad \underset{\sim}{E} = -\frac{\mu}{c}\dot{\underset{\sim}{A}} \tag{5}$$

where $\underset{\sim}{A}$ is any solution of

$$\nabla \times \left[\frac{1}{\rho}\nabla \times (\mu\underset{\sim}{A})\right] + k\mu\sigma\dot{\underset{\sim}{A}} = 0, \tag{6a}$$

subject only to the auxilary condition

$$\nabla \cdot (\mu\sigma\underset{\sim}{A}) = 0 \tag{6b}$$

(Here we neglect static magnetic fields.) Our choice of the

vector potential is such as to include the potential of the free charge distribution, namely, from (2),

$$-4\pi\epsilon = \nabla\cdot\left(\frac{K\mu}{c}\dot{\underline{A}}\right) \quad . \tag{7}$$

In terms of $\underline{A}$ we list below the boundary conditions appropriate to the transition surface separating two media $M_1(K_1, \mu_1, \sigma_1)$ and M_2. From the continuity of the tangential components of $\underline{E}$ and $\underline{H}$ and the normal component of $\underline{B}$, we have

$$\begin{aligned} \hat{n} \times \Delta(\mu\underline{A}) &\equiv \hat{n} \times \left\{(\mu\underline{A})_2 - (\mu\underline{A})_1\right\} = 0 \\ \hat{n} \times \Delta\left(\frac{1}{\mu}\nabla \times \mu\underline{A}\right) &= 0 \\ \hat{n} \cdot \Delta(\nabla \times \mu\underline{A}) &= 0 \ . \end{aligned} \tag{8}$$

The charge density η residing on the transition surface may be expressed in terms of the discontinuity in $\underline{D}\cdot\hat{n}$, as well as in $\underline{J}\cdot\hat{n}$ by the conservation of charge. Thus we may write

$$-\hat{n}\cdot\Delta\left(\frac{K\mu}{c}\dot{\underline{A}}\right) = 4\pi\eta = \hat{n}\cdot\underline{D}_2\left[1 - \frac{K_1\sigma_2}{K_2\sigma_1}\right] , \tag{9}$$

where $\hat{n}$ is directed from medium 1 into medium 2. If medium 2 is an insulator the above reduces to

$$\hat{n}\cdot\left(\frac{K\mu}{c}\dot{\underline{A}}\right)_1 = 0, \quad -\hat{n}\cdot\left(\frac{K\mu}{c}\dot{\underline{A}}\right)_2 = 4\pi\eta \ . \tag{10}$$

Applying these equations to the mantle we set $\sigma = \sigma(\rho)$, where $\rho = r/R_c$ and R_c is the radius of the core. Hereafter we shall always take μ = constant. Under these conditions, standard <u>toroidal solutions</u> have the same form as in the homogeneous case (σ = constant), namely,

$$\begin{aligned} \underline{A} &= \nabla \times \underline{r}\psi = \nabla\psi \times \underline{r} \\ \nabla^2\psi &= k\mu\sigma\dot{\psi} . \end{aligned} \tag{11}$$

General <u>poloidal solutions</u> are unknown. These solutions, however, are of little interest in the study of the secular variation since they give rise to toroidal magnetic fields which are not observable at the earth's surface (Elsasser, 1950). Standard solutions of Eq. (11) are

$$\underline{A} = R_c\,\mathcal{R}_n(\rho, t)\nabla S_n^m(\theta, \phi) \times \underline{r}, \tag{12}$$

where $\mathcal{R}_n(\rho,t)$ satisfies the spherical Bessel differential equation, with variable σ,

$$\frac{\partial^2}{\partial\rho^2}(\rho\mathcal{R}_n) = \frac{\partial}{\rho\partial\rho}\left\{\rho^2\frac{\partial\mathcal{R}_n}{\partial\rho}\right\} = \left\{\frac{n(n+1)}{\rho^2} + k\mu\sigma R_c^2\frac{\partial}{\partial t}\right\}\mathcal{R}_n\rho. \tag{13}$$

$S_n^m(\theta,\phi)$ is the usual surface harmonic.

Outside the conductive medium σ is identically zero, and $\mathcal{R}_n$ is computed from the resulting homogeneous equation. Corresponding solutions ψ_n are, for $r \geq R_e$ (earth's radius),

$$\begin{aligned}\psi^e_{nm} &= R_e(n+1)\, C^e_{nm}(t)\left(\frac{r}{R_e}\right)^n S^m_n(\theta,\phi)\\ \psi^i_{nm} &= -R_e n C^i_{nm}(t)\left(\frac{r}{R_e}\right)^{-n-1} S^m_n(\theta,\phi),\end{aligned} \tag{14}$$

where $C^e_{nm}(t)$ and $C^i_{nm}(t)$ are arbitrary complex functions of time. The corresponding vector potentials are, for $r \geq R_e$,

$$\begin{aligned}\underset{\sim}{A}^e_{nm} &= R_e C^e_{nm}(t)\left(\frac{r}{R_e}\right)^n \nabla S^m_n(\theta,\phi) \times \underset{\sim}{r}\\ \underset{\sim}{A}^i_{nm} &= R_e C^i_{nm}(t)\left(\frac{r}{R_e}\right)^{-n-1} \nabla S^m_n(\theta,\phi) \times \underset{\sim}{r},\end{aligned} \tag{15}$$

the coefficients being chosen so as to satisfy the relations $\underset{\sim}{H} = \nabla \times \underset{\sim}{A} = -\nabla\psi$. Here $C^e_{nm}(t)$ represents the inducing field whereas $C^i_{nm}(t)$ corresponds to the induced field together with the field of internal origin.

For later reference, the components of $\underset{\sim}{A}$ and $\underset{\sim}{H}$ are listed below ($R_c \leq r \leq R_e$):

$$\begin{aligned}A_r &= 0 & H_r &= \rho^{-1}\sum_{n,m} n(n+1)\psi_{nm}\\ A_\theta &= \frac{R_c}{\sin\theta}\sum_{n,m}\frac{\partial\psi_{nm}}{\partial\phi} & H_\theta &= \rho^{-1}\sum_{n,m}\frac{\partial}{\partial\rho}\left(\rho\frac{\partial\psi_{nm}}{\partial\theta}\right)\\ A_\phi &= -R_c\sum_{n,m}\frac{\partial\psi_{nm}}{\partial\theta} & H_\phi &= \frac{\rho^{-1}}{\sin\theta}\sum_{n,m}\frac{\partial}{\partial\rho}\left(\rho\frac{\partial\psi_{nm}}{\partial\phi}\right).\end{aligned} \tag{16}$$

Outside the mantle it is more convenient to replace R_c by R_e and ρ by r/R_e, where they occur explicitly in (16).

III. Periodic Solutions of Mantle Equations

Aside from an insulating mantle, the simplest earth model is that of an infinite conductive medium surrounding the core. We wish to examine this model with the chief aim of determining roughly the distribution of the bulk of electrical conductivity in the mantle. Waves introduced at the core boundary are investigated as to their attenuation and phase retardation at a distance equal to the earth's radius, reflection of waves being neglected.

For the electrical conductivity we choose the three-parameter distribution

$$\sigma(\rho) = \sigma_0 \rho^{-\gamma} + \sigma_1 \rho^{-2} \tag{17}$$

Using this function, we make the following substituions in Eq. (13), (Compare Lahiri and Price, Eq. 5.3.)

$$\mathcal{R}_n = \rho^{-\frac{1}{2}} W_{\nu_n}, \quad \zeta = i^{3/2} (\omega k \mu R_c^2 \sigma_0)^{\frac{1}{2}}$$
$$\frac{\partial}{\partial t} = i\omega, \quad \rho^{1-\gamma/2} = \frac{|\gamma-2|}{2\zeta} z, \quad \gamma \neq 2 \tag{18}$$
$$\nu_n = 2\left[(n+\tfrac{1}{2})^2 - \zeta^2 \sigma_1/\sigma_0\right]^{\frac{1}{2}} / |\gamma-2|, \quad n = 1,2,3,\ldots,$$

and find that $W_\nu(z)$ obeys Bessel's differential equation of order ν_n and argument z. For simplicity, in these initial calculations we shall always take $\sigma_1 \equiv 0$.

In the computations we consider only the radial component $\dot{H}_r$ for a sinusoidal input wave. In terms of the constant coefficients $\dot{H}^m_{rn}$ of an expansion of $\dot{H}r$ at the core, we then write, from (16),

$$\frac{\partial}{\partial t} H_r(\rho,\theta,\phi,t) = e^{iwt} \sum_{n,m} B_n e^{-i\phi_n} \dot{H}^m_{rn} S^m_n \tag{19}$$

where

$$B_n e^{-i\phi_n} = \rho^{-3/2} \left\{ \frac{W_{\nu_n}(z)}{W_{\nu_n}(z_c)} \right\}$$

z_c denotes the value of z at $r=R_c$. B_n is the real <u>total attenuation</u> and ϕ_n the real <u>phase retardation</u>. Since, in Part I, $\sigma_1 \equiv 0$, it follows that ν_n is real. Accordingly, three cases arise depending upon whether γ is greater, equal, or less than 2.

Case I ($\gamma > 2$). The equation (18) connecting ρ and z shows that $\rho \to \infty$ implies $z \to o$. Since $|\underline{A}| = O(\rho^2)$ when $\sigma = 0$, it follows that for $\sigma_o > 0$, $\underline{A}$ must vanish to at least this order. Therefore W(z) must vanish to the appropriate order when $z \to o$. The only solution of Bessel's dif. eq. satisfying this condition is that of the first kind, the series expansion being regular over the whole cut plane. We, therefore, write, for large values of ρ,

$$\rho^{-\frac{1}{2}} \mathfrak{R}_n(\rho, t) = \tag{20}$$

$$e^{i\omega t} \rho^{-3/2} J_{\nu_n}(z) \sim \frac{|\zeta|^{\nu_n} e^{i(\omega t + 3\pi\nu_n/4)}}{\Gamma(1+\nu_n)\,|\gamma-2|^{\nu_n}} \rho^{-n-2} = O(\rho^{-n-2}).$$

Case II ($\gamma = 2$). This case is singular for the substitutions (18). Eq. (13), however, is homogeneous, and a direct integration gives the general solution

$$\rho^{-\frac{1}{2}} \mathfrak{R}_n(\rho, t) = C^{(1)} \exp\left\{ i\left[\omega t - b_n \log\rho\right] - \left[a_n + 3/2\right]\log\rho \right\} + C^{(2)} \exp\left\{ i\left[\omega t + b_n \log\rho\right] + \left[a_n - 3/2\right]\log\rho \right\}, \tag{21}$$

where

$$a_n = \sqrt{\left\{ \tfrac{1}{2}(n+\tfrac{1}{2})^2 + \tfrac{1}{2}\sqrt{\left[|\zeta|^4 + (n+\tfrac{1}{2})^4\right]} \right\}} \geqslant n+\tfrac{1}{2}$$

$$b_n = \sqrt{\left\{ -\tfrac{1}{2}(n+\tfrac{1}{2})^2 + \tfrac{1}{2}\sqrt{\left[|\zeta|^4 + (n+\tfrac{1}{2})^4\right]} \right\}} \geqslant 0.$$

We are interested only in the expanding wave front. The total attenuation B_n and phase retardation ϕ_n in Eq. (19) are therefore

$$\phi_n = b_n \log\rho \,, B_n = \rho^{-3/2 - a_n} \tag{22a}$$

For large $|\zeta|$, $a_n \doteq b_n \doteq |\zeta| 2^{-\frac{1}{2}}$ so that

$$\phi_n \doteq 2^{-\frac{1}{2}} |\zeta| \log\rho \tag{22b}$$

$$B_n \doteq \rho^{-3/2 - |\zeta| 2^{-\frac{1}{2}}}$$

For $|\zeta|$ small, $a_n \doteq (n+\tfrac{1}{2}) + |\zeta|^4 (2n+1)^{-3}$, $b_n \doteq |\zeta|^2/(2n+1)$ and therefore

$$\phi_n \doteq |\kappa|^2 (2n+1)^{-1} \log \rho$$
$$B_n \doteq \rho^{n-2-|\kappa|^4 (2n+1)^{-3}} \qquad (22c)$$

Case III ($\gamma < 2$). Referring to Eq. (18), we see that with $\gamma < 2, \rho \to \infty$ implies $|z| \to \infty$. Since the attenuation here is greater than in the two preceeding cases, it follows that W_ν must vanish as $|z| \to \infty$. From all the cylinder functions we must, therefore, choose one of the two Hankel functions since they alone vanish in the neighborhood of the point $z = \infty$. Consistent with our choice of κ and the positive time factor we therefore write, in terms of the Hankel function of the first kind,

$$\rho^{-1} \mathfrak{R}_n(\rho, t) = e^{i\omega t} \rho^{-3/2} H^{(1)}_{\nu_n}(z). \qquad (23)$$

For large $|z|$

$$H^{(1)}_{\nu_n}(z) \sim \left[\frac{2}{\pi z}\right]^{\frac{1}{2}} e^{i(z - \nu_n \pi/2 - \pi/4)}.$$

Therefore

$$B_n e^{-i\phi_n} \sim \rho^{\gamma/4 - 2} \cdot \exp\{-(1+i) 2^{\frac{1}{2}} |\kappa| (\rho^{1-\gamma/2} - 1)/|\gamma - 2|\}.$$

To investigate the effects of a material medium we define the physical attenuation C_n as the ratio of the total attenuation B_n to the geometrical attenuation G_n:

$$C_n = \frac{B_n}{G_n}, \quad G_n = \rho^{-n-2} \qquad (24)$$

In free space $C_n = 1$. Observe that in the asymptotic expressions in the above three cases C_n is (I) constant, (II) varies as ~~an inverse~~ power law, (III) varies as the complex of an exponential attenuation and a ~~direct~~ power law. In case I, the phase retardation is constant; the conductivity rapidly approaches zero and $\dot{\underline{H}}$ approaches the gradient of a scalar time dependent potential, the equipotential surfaces varying isochronously.

Tables I and II include the tabulated values of B_n and ϕ_n for the γ-values indicated. In the calculation we take

$$|\kappa| = 5.4986 \cdot 10^5 [\delta \text{yr/emu}]^{\frac{1}{2}}, \quad \omega = 2\pi/T$$
$$\delta = \sigma_0/T, \quad \rho^{-1} = R_c/R_e = 0.546875, \qquad (25)$$

TABLE I. TOTAL ATTENUATION B_n

$\gamma = 0.000$

δ	B_1	B_2	B_3	B_4	B_5	B_6	B_7	B_8	B_9	B_{10}	B_{11}	B_{12}
$.0^85$*	$.0^{10}3793$	$.0^{10}3731$	---	---	---	$.0^{10}3218$	---	---	---	---	---	---
$.0^83$	$.0^86425$	$.0^86291$	---	---	---	$.0^85188$	---	---	---	---	---	---
$.0^82$	$.0^61634$	$.0^61591$	---	---	---	$.0^61256$	---	---	---	---	---	---
$.0^81$	$.0^41105$	$.0^41065$	---	---	---	$.0^57607$	---	---	---	---	---	---
$.0^95$	$.0^32168$	$.0^32058$	---	---	---	$.0^31273$	---	---	---	---	---	---
$.0^93$	$.0^21091$	$.0^21020$	---	---	---	$.0^35457$	---	---	---	---	---	---
$.0^91$	.01128	.01003	---	---	---	$.0^23434$	---	---	---	---	---	---
$.0^{10}5$	.02830	.0241	---	---	---	$.0^2574$	---	---	---	---	---	---
$.0^{10}1$	.09160	.0664	---	---	---	$.0^2794$	---	---	---	---	---	---
$.0^{11}1$	.1523	---	---	---	---	---	---	---	---	---	---	---
$.0^{12}1$	.163	.089	---	---	---	$.0^280$	---	---	---	---	---	---

$\gamma = 2.000$

$.0^61$	$.0^{32}2518$	---	---	---	---	---	$.0^{32}2357$	---	---	---	---	---
$.0^71$	$.0^{10}2621$	$.0^{10}2581$	$.0^{10}2522$	$.0^{10}2446$	$.0^{10}2353$	$.0^{10}2243$	$.0^{10}2125$	$.0^{10}1995$	$.0^{10}1858$	$.0^{10}1717$	$.0^{10}1574$	$.0^{10}1430$
$.0^83$	$.0^51051$	---	---	---	---	---	$.0^67122$	---	---	---	---	$.0^63377$
$.0^91$	$.0^32367$	$.0^32253$	$.0^32090$	$.0^31890$	$.0^31664$	$.0^31425$	$.0^31185$	$.0^49573$	$.0^47501$	$.0^45700$	$.0^44203$	$.0^43006$
$.0^93$	$.0^26619$	$.0^26039$	$.0^25246$	$.0^24325$	$.0^23376$	$.0^22493$	$.0^21744$	$.0^21161$	$.0^37405$	$.0^34562$	$.0^32734$	$.0^31604$
$.0^91$	.03546	.03007	.02322	.01631	.01055	$.0^26429$	$.0^23765$	$.0^22151$	$.0^21211$	$.0^36753$	$.0^33745$	$.0^32066$
$.0^{10}1$	.1421	.08584	.04815	.02655	.01457	$.0^27980$	$.0^24368$	$.0^22390$	$.0^21307$	$.0^37151$	$.0^33911$	$.0^32140$
$.0^{11}1$	.1632	.08941	.04891	.02675	.01463	$.0^28000$	$.0^24375$	$.0^22393$	$.0^21308$	$.0^37156$	$.0^33913$	$.0^32140$
$.0^{12}1$	.1635	.08944	.04891	.02675	.01463	$.0^28000$	$.0^24375$	$.0^22393$	$.0^21308$	$.0^37156$	$.0^33913$	$.0^32140$

$\gamma = 9.440$

$.0^73$	$.0^61186$	---	---	---	---	---	$.0^77067$	---	---	---	---	$.0^72615$
$.0^72$	$.0^52381$	---	---	---	---	---	$.0^51161$	---	---	---	---	$.0^63144$
$.0^71$	$.0^31193$	$.0^31089$	$.0^49492$	0^47875	$.0^46325$	$.0^44923$	$.0^43727$	$.0^42754$	$.0^41991$	$.0^41411$	$.0^59818$	$.0^56723$
$.0^87$	$.0^35488$	---	---	---	---	---	$.0^31332$	---	---	---	---	$.0^41960$
$.0^83$	$.0^27542$	$.0^25962$	$.0^24474$	$.0^23220$	$.0^22237$	$.0^21510$	$.0^39935$	$.0^36396$	$.0^34040$	$.0^32510$	$.0^31536$	$.0^49281$
$.0^81$	.05138	.03540	.02322	.01466	$.0^28985$	$.0^25376$	$.0^83157$	$.0^21827$	$.0^21045$	$.0^35928$	$.0^33338$	$.0^31869$
$.0^93$	.1298	---	---	---	---	---	$.0^24221$	---	---	---	---	$.0^32112$
$.0^91$	.1586	.08786	.04827	.02650	.01453	$.0^27958$ 8000	$.0^24357$	$.0^22385$	$.0^21305$	$.0^37141$	$.0^33906$	$.0^32137$
$.0^{10}1$	.1635	.08942	.04891	.02675	.01463	$.0^28000$	$.0^24375$	$.0^22393$	$.0^21308$	$.0^37156$	$.0^33913$	$.0^32140$
$.0^{11}1$	.1635	.08944	.04891	.02675	.01463	$.0^28000$	$.0^24375$	$.0^22393$	$.0^21308$	$.0^37156$	$.0^33913$	$.0^32140$

$\gamma = 14.16$

$.0^75$	$.0^52212$	---	---	---	---	---	$.0^64807$	---	---	---	---	$.0^78822$
$.0^73$	$.0^44581$	$.0^43604$	$.0^42761$	$.0^42069$	$.0^41520$	$.0^41097$	$.0^57800$	$.0^55467$	$.0^53784$	$.0^52582$	$.0^51752$	$.0^51174$
$.0^71$	$.0^23270$	$.0^22354$	$.0^21653$	$.0^21135$	$.0^37666$ 553	$.0^35075$	$.0^33316$	$.0^32139$	$.0^31363$	$.0^48597$	$.0^45368$	$.0^43322$
$.0^83$	.03740	.02448	.01565	$.0^29802$	$.0^26034$	$.0^23660$	$.0^22187$	$.0^21297$	$.0^37603$	$.0^34417$	$.0^32547$	$.0^31463$
$.0^81$	.1083	.06453	.03786	.02166	.01231	$.0^26940$	$.0^23887$	$.0^22167$	$.0^21203$	$.0^36661$	$.0^33680$	$.0^32029$
$.0^91$	.1626	.08906	.04891	.02668	.01460	$.0^27988$	$.0^24369$	$.0^22390$	$.0^21307$	$.0^37150$	$.0^33913$	$.0^32139$
$.0^{10}1$	.1635	.08944	.04891	.02675	.01463	$.0^28000$	$.0^24375$	$.0^22393$	$.0^21308$	$.0^37156$	$.0^33913$	$.0^32140$
$.0^{11}1$	.1635	.08944	.04891	.02675	.01463	$.0^28000$	$.0^24375$	$.0^22393$	$.0^21308$	$.0^37156$	$.0^33913$	$.0^32140$

$\gamma = 18.90$

$.0^61$	$.0^51454$	$.0^51079$	$.0^67889$	$.0^65688$	$.0^64051$	$.0^62854$	$.0^61990$	$.0^61375$	$.0^79421$	$.0^76404$	$.0^74321$	$.0^72910$
$.0^75$	$.0^46845$	---	---	---	---	---	$.0^57368$	---	---	---	---	$.0^88817$
$.0^73$	$.0^36950$	$.0^34866$ 70	$.0^33279$	$.0^32216$	$.0^31465$	$.0^49634$	$.0^46274$	$.0^44049$	$.0^42593$	$.0^41647$	$.0^41040$	$.0^56519$
$.0^71$	.01384	$.0^28984$	$.0^25748$	$.0^23823$ 963	$.0^22269$	$.0^21403$	$.0^38601$	$.0^35229$	$.0^33155$	$.0^31891$	$.0^31126$	$.0^46666$
$.0^85$	.04195	.02618	.01611	$.0^29871$ 963	$.0^25890$	$.0^83508$	$.0^22072$	$.0^81214$	$.0^37065$	$.0^34060$	$.0^32349$	$.0^31344$
$.0^81$	.1393	.07934	.04400	.02451	.01359	$.0^27524$	$.0^24153$	$.0^22288$	$.0^21259$	$.0^36920$	$.0^33797$	$.0^32086$
$.0^91$	.1632	.08931	.04886	.02673	.01462	$.0^27995$	$.0^24373$	$.0^22392$	$.0^21308$	$.0^37153$	$.0^33912$	$.0^32140$
$.0^{10}1$	.1635	.08944	.04891	.02675	.01463	$.0^28000$	$.0^24375$	$.0^22393$	$.0^21308$	$.0^37156$	$.0^33913$	$.0^32140$
$.0^{11}1$	.1635	.08944	.04891	.02675	.01463	$.0^28000$	$.0^24375$	$.0^22393$	$.0^21308$	$.0^37156$	$.0^33913$	$.0^32140$

$\gamma = 28.33$

$.0^63$	$.0^62588$	$.0^61749$	$.0^61173$	$.0^77809$	$.0^75167$	$.0^73398$	$.0^72222$	$.0^71446$	$.0^89360$	$.0^86097$	$.0^83869$	$.0^82470$
$.0^62$	$.0^54412$	$.0^52938$	$.0^51942$	$.0^51276$	$.0^68398$	$.0^65407$	$.0^63491$	$.0^62244$	$.0^61435$	$.0^79244$	$.0^75802$	$.0^73667$
$.0^61$	$.0^31708$	$.0^31106$	$.0^47123$	$.0^44559$	$.0^42900$	$.0^41835$	$.0^41155$	$.0^67230$	$.0^64511$	$.0^62802$	$.0^61733$	$.0^51068$
$.0^73$	$.0^88008$	$.0^24965$	$.0^23057$	$.0^21871$	$.0^21138$	$.0^36891$	$.0^34151$	$.0^32489$	$.0^31486$	$.0^48838$	$.0^45237$	$.0^43092$
$.0^71$	.04938	.02940	.01739	.01022	$.0^25977$	$.0^23477$	$.0^22014$	$.0^81161$	$.0^36670$	$.0^33817$	$.0^32177$	$.0^31238$
$.0^83$	.1264	.07142	.04015	.02248	.01254	$.0^26978$	$.0^23873$	$.0^82146$	$.0^81187$	$.0^36553$	$.0^33614$	$.0^31991$
$.0^81$	.1579	.08681	.04768	.02616	.01435	$.0^27867$	$.0^24311$	$.0^82361$	$.0^81293$	$.0^37088$	$.0^33844$	$.0^32122$
$.0^91$	.1635	.08942	.04890	.02674	.01463	$.0^27999$	$.0^24374$	$.0^22393$	$.0^21308$	$.0^37155$	$.0^33913$	$.0^32140$
$.0^{11}1$	.1635	.08944	.04891	.02675	.01463	$.0^28000$	$.0^24375$	$.0^22393$	$.0^21308$	$.0^37156$	$.0^33913$	$.0^32140$

* The notation $.0^85$ denotes 5×10^{-9}.

TABLE 2. PHASE RETARDATION ϕ_n

γ = 0.000

δ	ϕ_1	ϕ_2	ϕ_3	ϕ_4	ϕ_5	ϕ_6	ϕ_7	ϕ_8	ϕ_9	ϕ_{10}	ϕ_{11}	ϕ_{12}
$.0^85$*	22.773	22.756	----	----	----	22.61	----	----	----	----	----	----
$.0^83$	17.64	17.61	----	----	----	17.43	----	----	----	----	----	----
$.0^82$	14.395	14.37	----	----	----	14.15	----	----	----	----	----	----
$.0^81$	10.17	10.14	----	----	----	9.832	----	----	----	----	----	----
$.0^95$	7.180	7.132	----	----	----	6.73	----	----	----	----	----	----
$.0^93$	5.550	5.491	----	----	----	5.0	----	----	----	----	----	----
$.0^91$	3.174	3.08	----	----	----	----	----	----	----	----	----	----
$.0^{10}5$	2.216	2.1	----	----	----	----	----	----	----	----	----	----
$.0^{10}1$	.9163	----	----	----	----	----	----	----	----	----	----	----
$.0^{11}1$	.2013	----	----	----	----	----	----	----	----	----	----	----
$.0^{12}1$	.03007	----	----	----	----	----	----	----	----	----	----	----
						γ = 2.000						
$.0^61$	74.16	----	----	----	----	----	74.09	----	----	----	----	----
$.0^71$	23.44	23.43	23.40	23.37	23.33	23.29	23.23	23.17	23.10	23.03	22.94	22.85
$.0^81$	7.388	7.340	7.267	7.171	7.054	6.916	6.760	6.587	6.400	6.202	5.996	5.785
$.0^91$	2.259	2.116	1.924	1.713	1.508	1.328	1.176	1.050	.946	.860	.787	.725
$.0^{10}1$	.525	.355	.258	.202	.165	.140	.121	.105	.096	.085	.074	.074
$.0^{11}1$	.063	.037	.027	.018	.016	.012	.012	.01	.01	.01	.01	.01
$.0^{12}1$	.006	.00	.00	.00	.00	.00	.00	.00	.00	.00	.00	.00
						γ = 9.440						
$.0^73$	16.22	----	----	----	----	----	15.58	----	----	----	----	14.81
$.0^71$	9.310	9.176	9.126	8.863	8.700	8.535	8.369	8.203	8.038	7.875	7.715	7.556
$.0^87$	7.729	----	----	----	----	----	6.742	----	----	----	----	5.947
$.0^83$	4.880	4.704	4.529	4.357	4.189	4.026	3.869	3.718	3.572	3.433	3.300	3.172
$.0^91$	2.545	2.366	2.197	2.040	1.896	1.765	1.646	1.538	1.441	1.354	1.275	1.204
$.0^93$	1.055	----	----	----	----	----	.5321	----	----	----	----	.3706
$.0^91$	.3802	.3221	.2770	.2436	.2175	.1963	.1789	.1643	.1519	.1412	.1320	.1238
$.0^{10}1$	.0385	.0323	.0278	.0244	.0218	.0197	.0179	.0164	.0153	.0141	.0132	.0124
$.0^{11}1$	$.0^2389$	$.0^2327$	$.0^2281$	$.0^2247$	$.0^2220$	$.0^2199$	$.0^2181$	$.0^2166$	$.0^2154$	$.0^2143$	$.0^2134$	$.0^2125$
$.0^{12}1$	$.0^3389$	$.0^3327$	$.0^3281$	----	----	----	----	----	----	----	----	$.0^3125$
						γ = 14.16						
$.0^75$	13.66	----	----	---	---	----	12.93	----	----	----	----	12.34
$.0^73$	10.45	10.33	10.21	10.09	9.966	9.846	9.727	9.609	9.493	9.377	9.263	9.150
$.0^72$	8.430	----	----	----	----	----	----	----	----	----	----	----
$.0^71$	5.790	5.666	5.545	5.426	5.307	5.194	5.081	4.971	4.862	4.756	4.653	4.551
$.0^83$	2.898	2.778	2.663	2.551	2.444	2.341	2.245	2.150	2.061	1.977	1.897	1.821
$.0^81$	1.388	1.277	1.178	1.090	1.012	0.9432	.8818	.8271	.7020	.7344	.6950	.6594
$.0^91$	.1635	.1446	.1295	.1173	.1072	.09871	.09145	.08518	.07926	.07492	.07060	.06681
$.0^{10}1$	.01639	.01448	.01297	.01173	.01074	$.0^29882$	$.0^29155$	$.0^28527$	$.0^27979$	$.0^27498$	$.0^27072$	$.0^26691$
$.0^{11}1$	$.0^21640$	$.0^21448$	$.0^21297$	$.0^21174$	$.0^21074$	$.0^39882$	$.0^39155$	$.0^38527$	$.0^37979$	$.0^37498$	$.0^37072$	$.0^36691$
						γ = 18.90						
$.0^61$	14.00	13.92	13.83	13.74	13.65	13.56	13.47	13.38	13.29	13.20	13.12	13.03
$.0^71$	4.055	3.966	3.878	3.795	3.706	3.625	3.544	3.465	3.387	3.311	3.237	3.164
$.0^85$	2.703	2.615	2.529	2.447	2.365	2.286	2.211	2.138	2.067	2.013	1.934	1.872
$.0^81$	.8407	.7660	.7184	.6684	.6232	.5855	.5509	.5200	.4922	.4671	.4444	.4237
$.0^91$	.0898	.0816	.0748	.0690	.0641	.0598	.0561	.0528	.0498	.0472	.0448	.0426
$.0^{10}1$	$.0^2899$	$.0^2817$	$.0^2749$	$.0^2690$	$.0^2640$	$.0^2598$	$.0^2561$	$.0^2528$	$.0^2499$	$.0^2472$	$.0^2448$	$.0^2427$
$.0^{11}1$	$.0^390$	$.0^382$	$.0^375$	$.0^369$	$.0^364$	$.0^360$	$.0^356$	$.0^353$	$.0^350$	$.0^347$	$.0^345$	$.0^343$
$.0^{12}1$	$.0^49$	$.0^48$	$.0^47$	$.0^47$	$.0^46$	$.0^46$	$.0^46$	$.0^45$	$.0^45$	$.0^45$	$.0^44$	$.0^44$
						γ = 28.33						
$.0^63$	15.70	15.64	15.58	15.52	15.46	15.40	15.34	15.28	15.21	15.15	15.09	15.03
$.0^62$	12.72	12.66	12.60	12.55	12.49	12.43	12.37	12.31	12.25	12.20	12.14	12.08
$.0^61$	8.851	8.792	8.732	8.675	8.617	8.559	8.502	8.445	8.388	8.332	8.276	8.219
$.0^73$	4.621	4.562	4.505	4.447	4.391	4.335	4.280	4.225	4.171	4.117	4.065	4.013
$.0^71$	2.449	2.359	2.335	2.279	2.225	2.172	2.119	2.069	2.019	1.971	1.923	1.878
$.0^83$	1.053	1.002	.9542	.9102	.8695	.8318	.7968	.7643	.7341	.7059	.6797	.6552
$.0^81$	.3857	.3620	.3410	.3222	.3054	.2901	.2722	.2638	.2523	.2417	.2301	.2231
$.0^91$	.03914	.03665	.03445	.03250	.03075	.02919	.02778	.02650	.02533	.02426	.02328	.02237
$.0^{11}1$	$.0^33916$	$.0^33666$	$.0^33446$	$.0^33251$	$.0^33076$	$.0^32920$	$.0^32779$	$.0^32650$	$.0^32534$	$.0^32426$	$.0^32328$	$.0^32237$

* The notation $.0^85$ denotes 5×10^{-9}.

where σ_0 is measured in emu and T in years. ζ is dimensionless. Standard asymptotic expansions of $H_\nu^{(1)}$ and J_ν were employed for those larger values of δ for which the series expansions failed to converge rapidly (approximately 15 terms). The values of B_n and ϕ_n are, in general, accurate to four significant figures. Computational errors were checked only by continuity of graphs. The values of γ = 9.440, 14.16, 18.90, 28.33 were chosen such that the conductivity at the 700-km depth would be 10^{-2}, 10^{-3}, 10^{-4}, 10^{-6} times σ_0, the value at the core surface.

Figures 1 to 5 show plots of the first twelve coefficients over the appropriate range δ, or $|\zeta|$, as shown. The left-hand horizontal portion of each curve indicates the geometrical attenuation. Observe that with increasing γ, the curves are shifted to the right. That is, for a constant period of vibration and total attenuation, an increase in γ requires an increase in σ_0. The fact that the first and twelfth harmonics approach each other, as δ increases, clearly shows that C_n increases with increasing order of harmonic---lower order harmonics are physically attenuated more than those of higher order.

In Fig. 6 the total attenuation of the first harmonic is plotted as a function of γ throughout the range 0 to 35.

Fig. 7 shows the physical attenuation for the first, seventh, and twelfth harmonics for values of γ = 2.000, 9.440, and 28.33. With increasing γ each family becomes more compact and is displaced towards the right.

Fig. 8 shows the relative physical attenuations C_7/C_1 and C_{12}/C_1. For example, for γ = 9.440 and $\delta = 10^{-8}$ emu/yr., we see that the first harmonic is attenuated approximately 44 times the twelfth harmonic.

The phase retardation ϕ_n is plotted in Fig. 12 for γ-values equal to 2.000, 9.440, 18.90 and 28.33. The travel time required for waves leaving the core to reach the earth's surface is obtained from the expression

$$t = \phi_n T/2\pi, \qquad (26)$$

where T is the wave period. For example, for γ = 9.440 and $\delta = 10^{-8}$ emu/yr., we find for the first and twelfth harmonics, t_1 = 1.48 yrs., t_{12} = 1.20 yrs. so that the first

harmonic would arrive approximately 3 1/3 months after the twelfth harmonic. This quasi-dispersive effect occurs for a pure sinusoidal source.

IV. Equivalent Conductivity

The utility of an equivalent δ (equivalent conductivity) lies in the fact that calculations involving the earth's mantle may be simplified by a choice of the radial dependence of the electrical conductivity, such as a constant or an inverse square law. We next establish such an equivalence for later reference.

For a harmonic of given degree, Fig. 9 shows that curves B_n, for different values of γ, are nearly "parallel". This implies that one may establish, for each harmonic, an equivalent δ, δ_c, valid over a reasonably large B_n-interval by a horizontal translation of that B_n-curve for which $\gamma=0$ (constant electrical conductivity). The translations $\log_{10}\tau = \log_{10}\delta - \log_{10}\delta_c$ of the zero-curve to any chosen γ-curve, for various constant physical attenuations, are shown in Fig. 10. Curves I, II, III, for $n = 6$, correspond to constant physical attenuations 0.800, 0.500, and 0.204. The attenuations of the first harmonic, corresponding to these constant attenuations, are shown in Fig. 9 by the curves I', II', III', and the geometric means between the extreme points ($\gamma = 0$ and $\gamma = 35$) of these curves are shown by curves I", II", III". Here the physical attenuations are C_1 = 0.37, 0.18 and 0.061. The displacements $\log \delta/\delta_c$ are shown in Fig. 10, for n = 1, for the curves I", II", III", together with the curve III. Curve III represents a total attenuation of amount $B_n = 1.63 \times 10^{-3}$, the corresponding physical attenuations being $C_1 = 0.010$ and $C_6 = 0.204$. In Fig. 10, observe that the curves for n = 6 are grouped closer together than those for n = 1. Curves for n greater (lesser) than 6 lie below (above) those for n = 6. An inversion of the curves, n = 6, occurs at $\gamma \doteq 8.5$, curves I and III intersecting curve II. The results for n = 12 have not been included here. However, from the graphs of the physical attenuation, Fig. 7, one may expect this family to be quite compact and to lie somewhat closer to the family n = 6 than does the family n = 1.

Data scaled from Fig. 9 is given below. The tabulated values indicate $\log_{10}\gamma$. The last three columns pertain to the family n = 1.

TABLE 3

γ	I	II	III	I"	II"	III"
2.000	0.407	0.38	0.337	0.435	0.38	0.35
5.000	-----	----	-----	1.04	0.93	0.84
9.440	1.25	1.24	1.22	1.61	1.48	1.38
14.16	1.50	1.50	1.51	1.98	1.85	1.76
18.90	1.68	1.70	1.71	2.25	2.12	2.03
28.33	1.99	2.00	2.01	2.59	2.47	2.14
35.00	----	----	----	2.78	2.68	2.59

In general, different attenuation curves cannot be made to coincide everywhere by a relative horizontal translation. An attenuation curve $B_n(\delta;\gamma)$ coincides with the translated zero curve $B_n(\tau\,\delta_c;0)$ only in the δ-neighborhood about the point of intersection of these curves with the specified physical attenuation which characterizes τ. To indicate the error incurred by using the translated zero-curve, Fig. 11b shows, roughly, the maximum and minimum ratio of $B_n(\delta;\gamma)$ to $B_n(\tau\delta_c;0)$, taken along the same δ-ordinate for both n = 1 and n = 6, over the range of attenuation in Fig. 9. Throughout the γ-range indicated, the maximum error occurs at approximately the same value of total attenuation. These values are indicated by the parenthesized quantities in Fig. 11b. τ corresponds to curve III.

Fig. 11a again illustrates the maximum and minimum values of the ratio $B_n(\delta;\gamma)$ to $B_n(\tau\delta_c;0)$ for the constant attenuation shown by curve III. Here, however, the roles for n = 1 and n = 6 were interchanged in computing τ. Thus the curves marked n = 1 (n = 6) in Fig. 11a indicate the maximum error in the first (sixth) harmonic due to the employ of the translated δ computed from the sixth (first) harmonic.

We postulate that the secular field, $\dot{H}_r(R_e,\theta,\phi,t)$ would require twelve harmonics for a representation with an error not larger than, say, 3 or 4%. The translation of an inter-

mediary harmonic, say n = 6, would therefore be expected to represent, very roughly, the translation of the representation of the whole secular field. Since the τ-curves for n = 6, Fig. 10, are quite compact, we arbitrarily choose curve II in the approximation of the equivalent δ, δ_c. From the Maclaurin expansion $\log_{10}\tau = a\gamma + b\gamma^2 + c\gamma^3 + \ldots$, we may write

$$\sigma_c = T_c\delta_c = \sigma\frac{T_c}{T}\exp\left\{-(a\gamma+b\gamma^2+c\gamma^3+\ldots)\log_e 10\right\}, \qquad (27)$$

where a,b,c,..., are determined from Table 3. For curves II and II" the first few coefficients are tabulated below. For these curves, the points γ= 2.000, 9.440, 18.90, 28.33 and γ= 2.000, 14.16, 28.33 were employed.

	CURVE II	CURVE II"
a	0.211	0.202
b	-0.0113	-0.00599
c	0.000324	6.89×10^{-5}
d	-3.60×10^{-6}	----------

Of especial interest is the value γ= 5.45(cf. Eq.38). From (27), with T_c= T, we compute the equivalent conductivity in terms of the conductivity σ_o at the core-mantle boundary

$$\begin{aligned} \sigma_c &= 0.1370\ \sigma_o, \quad \text{Curve II(n = 6)} \\ \sigma_c &= 0.1164\ \sigma_o, \quad \text{Curve II" (n = 1)} \end{aligned} \qquad (28)$$

In Part II we shall make use of (28) to compute σ_o from a direct computation of σ_c.

V. Computation of Electrical Conductivity

If one neglects reflections at the earth's surface, the electrical conductivity of the mantle may be estimated by a method which replaces the time averaged squared field of $\dot{H}_r$ at the core by a properly weighted static distribution. The method has the advantage that a knowledge of the absolute magnitude of the field at the core is unnecessary; only the relative field is required. We first consider a general expansion of $\dot{H}_r$ in the form (29)

$$\dot{H}_r(\rho, \theta, \phi, t) = \sum_{n=1}^{\infty} B_n e^{-i\phi n} \sum_{m=0}^{n} P_n^m(\cos\theta)\left[a_{nm}\cos m\phi + b_{nm}\sin m\phi\right],$$

where, from Eq. (16), a_{nm} and b_{nm} are proportional to $\mathring{V}_n(1,t)$ and

$$B_n(\rho,t)e^{-i\phi_n(\rho,t)} = \rho^{-1}\frac{\mathring{V}_n(\rho,t)}{\mathring{V}_n(1,t)} \quad .$$

B_n and ϕ_n are again the real total attenuation and real phase retardation. Making use of the usual orthogonality relations, the surface average of $|\mathring{H}_r|^2$ is

$$h^2 = \sum_{n=1}^{\infty} \frac{B_n^2}{2n+1}\left[|a_{no}|^2 + \sum_{m=1}^{n}\left(\frac{|a_{nm}|^2 + |b_{nm}|^2}{2}\right)\frac{(n+m)!}{(n-m)!}\right]. \qquad (30)$$

Observational values of $B_n(R_e/R_c,t)a_{nm}$ and $B_n b_{nm}$ are provided by Vestine (ref. 6, p.42). In terms of associated Legendre polynomials, his analysis is written

$$\mathring{H}_r = \sum_{n=1}^{\infty}\frac{n+1}{n}\left\{A_n^o P_n + \sum_{m=1}^{n}\left[\frac{2(n-m)!}{(n+m)!}\right]^{\frac{1}{2}} P_n^m(\cos\theta)\left[A_n^m \cos m\phi + B_n^m \sin m\phi\right]\right\}, \qquad (31)$$

where A_n^m and B_n^m are tabulated. According to (31) the time average of h^2 is

$$h_t^2 = \sum_{n=1}^{\infty}\frac{V_{nt}}{2n+1}, \quad V_{nt} = \left(\frac{n+1}{n}\right)^2\left[|A_n^o|_t^2 + \sum_{m=1}^{n}\left(|A_n^m|_t^2 + |B_n^m|_t^2\right)\right]. \qquad (32)$$

The subscript t denotes the time average. $\sqrt{V_{nt}}$ is tabulated below, Table 4, for n = 1,2,...,6. The time average was taken only over the four ten year epochs 1912.5, 1922.5, 1932.5 and 1942.5. The values of A_n^m or B_n^m found separately from

TABLE 4

n	$V_{nt}^{\frac{1}{2}}$ γ/yr.	n	$V_{nt}^{\frac{1}{2}}$ γ/yr.
1	46.58	4	51.01
2	89.67	5	56.17
3	69.44	6	33.31

Vestine's $\dot{X}$ and $\dot{Y}$ analyses were averaged algebraically. The significance of some of these coefficients is somewhat in doubt because of the rather large discrepencies found in his two values for the same coefficient. The error in $V_{nt}^{\frac{1}{2}}$ is further augmented by the limited data; the epochs for which there exist reliable date cover only 40 years. To supplement Table 4, a straight

line ($y = -12.26n + 110.3$) was fitted by the method of least squares to the points $(V_{nt}^{\frac{1}{2}}, n)$ for $n = 2,3,4,5,6$. These results, together with the first term of Table 4, are shown in Table 5. Plots of $V_n^{\frac{1}{2}}$, for each epoch, and $V_{nt}^{\frac{1}{2}}$ are shown in Fig. 15a.

TABLE 5

n	y(γ/yr.)	n	y(γ/yr.)
1	46.58	4	61.28
2	85.80	5	49.02
3	73.54	6	36.76

Evidently, for the particular time interval represented by these plots, the activity of the secular field successively diminishes.

We next compare (32) with the time average of h^2 in (30). Since the two expressions are identical, term by term, we then have, at the earth's surface,

$$B_n = V_{nt}^{\frac{1}{2}} \left\{ |a_{no}|_t^2 + \sum_{m=1}^{n} \frac{1}{2} \left[|a_{nm}|_t^2 + |b_{nm}|_t^2 \right] \frac{(n+m)!}{(n-m)!} \right\}^{-\frac{1}{2}} \qquad (33)$$

At the core, $B_n = 1$, $\phi_n = 0$ so that $\dot{H}_r$ is expressed in terms of a_{nm} and b_{nm}. Various criteria are available for estimating the quantities a_{nm}, b_{nm}. These will be discussed shortly. The ratio B_i/B_j of the total attenuation of the i^{th} to the j^{th} solid harmonic is now compared with the same ratio calculated from Table I. Figures 13, 14 and 15 show all these calculated ratios for $n = 1,2,\ldots,6$. Also included is the ratio B_{12}/B_1. In these graphs, a specified value of B_i/B_j intersects the various γ-curves at critical values of δ. Curves for these points on a γ-δ coordinate system for various number pairs (i,j) may be expected to intersect in a small region of the plane (ideally, at a single point if only one frequency were present; increasing the frequency would increase the ordinate of this point.) The values of γ and δ appropriate to the mantle are then read off the graph.

We now return to the coefficients a_{nm} and b_{nm}. Because of the slow convergence of (29) at the core, we choose as a first, rough approximation

$$|a_{ij}|_t^2 \left[\frac{2}{2I+1} \frac{(i+j)!}{(i-j)!} \right] = |a_{kl}|_t^2 \left[\frac{2}{2k+1} \frac{(k+l)!}{(k-l)!} \right],$$

for all i,j,k,l. Accordingly, the ratios B_i/B_j in Eq. (33) are

$$B_i/B_j = \left[\frac{(j+1)\ V_{it}}{(i+1)\ V_{jt}}\right]^{1/2}. \qquad (34)$$

Further refinements in these ratios will now be obtained from a consideration of the magnetic field at the core.

The bulk of the magnetic topography, for $\dot{H}_r$, has been described in terms of an extensive system of ridges, in motion, the function $\dot{H}_r$ varying rapidly as we traverse the core surface (ref.1). The cross-sectional shape of a typical ridge at present is unknown. The ridge half-width, however, is sufficiently small (3 to 10 degrees of arc) to make the expansion (29), at the core, quite insensitive to the cross-sectional shape. To illustrate this insensitivity we tabulate the first few coefficients of a zonal harmonic expansion of three simple functions of axial symmetry.

$$f_1 = \frac{\cos\theta - \cos\alpha}{1 - \cos\alpha}, \quad \theta \leqslant \alpha; \quad f_1 = 0, \quad \alpha \leqslant \theta \leqslant \pi$$

$$f_2 = 1, \quad \theta \leqslant \alpha; \quad f_2 = 0, \quad \alpha < \theta \leqslant \pi$$

$$f_3 = \frac{1-\cos\theta}{1-\cos\alpha}, \quad \theta \leqslant \alpha; \quad f_3 = 0, \quad \alpha < \theta \leqslant \pi$$

A_i	$f_1(\alpha=15^\circ)$	$f_1(\alpha=30^\circ)$	$f_2(\alpha=15^\circ)$ $\times 0.500$	$f_2(\alpha=30^\circ)$ $\times 0.500$	$f_3(\alpha=30^\circ)$
A_0	0.00852	0.0335	0.00852	0.0335	0.0335
A_1	0.0253	0.0960	0.0251	0.0939	0.0915
A_2	0.0412	0.146	0.0404	0.135	0.125
A_3	0.0556	0.177	0.0537	0.150	0.124
A_4	0.0683	0.186	0.0641	0.137	0.0881
A_5	0.0787	0.174	0.0715	0.0993	0.0251
A_6	0.0865	0.144	0.0755	0.0467	-0.0502
A_7	0.0916	0.102	0.0755	-0.0088	-0.120
A_8	0.0938	0.0564	------	------	-----
A_9	0.0932	0.0138	------	------	-----
A_{10}	0.0900	-0.0197	------	------	-----

The examples serve to illustrate the increase of insensitivity to cross-sectional shape with decreasing half-angle. For functions of half-angle 5°-10° the effect is considerably enhanced.

Neglecting the cross-sectional shapes of the ridges, it follows that the quantities $|a_{nm}|_t^2$ and $|b_{nm}|_t^2$ in (33) are closely approximated by the SURFACE AVERAGE OF THE corresponding SQUARED coefficients computed from a properly weighted static distribution which varies rapidly over the core. For a purely <u>random distribution</u> of the function

$$\dot{H}_r(R_c,\theta) = \dot{H}_{ro}\sum_n A_n P_n(\cos\theta) \qquad (35)$$

of axial symmetry, we make use of the Legendre addition theorem (Eq. 4, ref. 1) and compute the ratio

$$B_i/B_j = |A_j/A_i| \cdot (V_{it}/V_{jt})^{\frac{1}{2}} \qquad (36)$$

which, again, is independent of the magnitude of the field at the core. For small half-angles $|A_i| \doteq |A_j|$ so that (36) does not differ appreciably from (34).

Our choice of a random distribution seems quite justified. Vestine's secular variation maps show a relatively rapid regional motion of the ridges superimposed upon the general westerly drift. Taken over a few hundred years one would therefore not expect a ϕ- dependence in the time average of $|\dot{H}_r|^2$. Likewise, there is, at most, a small θ-dependence; the 4 or 5 active localized regions at the core occur, evidently, quite randomly. [If, however, these regions remain within the latitudes , say 75°N and 75°S, the field at the earth's surface would still be large over the polar caps and would therefore tend to mask any small θ-dependence.] The θ-dependence at the earth's surface may be illustrated by the line integral of $|\dot{H}_r|_t^2$ along the parallels of latitude:

$$f(\theta) = \left[\frac{1}{2\pi}\int_0^{2\pi} |\dot{H}_r|_t^2 \, d\phi\right]^{\frac{1}{2}}$$

Table 6 below shows $f(\theta)$ computed from Vestine's data (ref. 5, pp. 304-311) for 10° intervals of latitude. The time average includes only the four available epochs, which are insufficient to depict the expected equatorial symmetry.

For a comparison with the random distribution, Eq.(36), the following interesting model illustrates a θ-dependence: Two identical functions (35) of axial symmetry and half-angle α

are placed adjacent to each other at the equator in a fixed east-west orientation, their centers being separated by an arc 2α. One function is then reflected at the core surface ($A_n \rightarrow -A_n$) such that their common point is a point of reflection. Denote the (θ,ϕ) coordinates of the centers of these functions by the subscripts 1 and 2. This "dipole" is then distributed over the core surface according to the restraining equations

$$\theta_1 = \theta_2 = \theta, \quad \phi_1 = \phi + \alpha, \quad \phi_2 = \phi - \alpha .$$

At the poles the centers coincide and the functions just cancel.

TABLE 6

θ	$f(\theta)$ γ/yr.	θ	$f(\theta)$ γ/yr.
0	39.5	180	53.4
10	39.7	170	68.9
20	40.8	160	88.8
30	46.3	150	92.9
40	56.2	140	81.2
50	59.1	130	65.3
60	55.8	120	54.6
70	53.1	110	55.2
80	56.8	100	60.0
90	60.9		

Using the Legendre addition theorem we compute the ratios of total attenuation

$$B_i/B_j = \Delta_{ij} \cdot \left|A_j/A_i\right| \cdot (V_{it}/V_{jt})^{\frac{1}{2}} , \qquad (37)$$

where

$$\Delta_{ij} = \left[\frac{(2i+1)}{(2j+1)} \cdot \frac{(2j+1)\sin\alpha - \sin(2j+1)\alpha}{(2i+1)\sin\alpha - \sin(2i+1)\alpha}\right]^{\frac{1}{2}}$$

If Δ_{ij} were unity, (37) would be equal to (36).

Figs. 15b to 15i show the plots of the ratios B_i/B_j computed from Eqs. (34), (36), and (37), using Tables 4 and 5. The quantities A_n in (36) and (37) were taken from Appendix A, ref. 1, for the appropriate half-angles α indicated in the figures. The figures pertaining to (37) have been included only for their heuristic value; the static distribution at

the core is too unrealistic. In all the figures, except 15d and 15e, the region of greatest convergence of the curves was roughly estimated by locating graphically the minimum of the relative mean deviations of the points of intersection of the curves with the γ-ordinates. The relative mean deviations were computed for increments of γ=1.25. The average critical-values of δ and γ are (1 ohm^{-1} m$^{-1}\equiv 10^{-11}$ emu)

$$\gamma_{av.} = 5.45 \qquad \delta_{av.} = 7.20 \times 10^{-10} \text{emu/yr.} \qquad (38)$$

Here the data of Fig. 15i was weighted by a factor of 2. If it is assumed that Vestine's coefficients A_n^m and B_n^m are representative of an average period of 50 years, the electrical conductivity at the core -mantle boundary and the equivalent conductivity from Eq. (28), are

$$\sigma_o = 50 \text{ yr} \times \delta_{av.} = 3.60 \times 10^{-8} \text{emu}, \quad \sigma_c = 4.93 \times 10^{-9} \text{emu}. \qquad (39)$$

~~A lower limit of σ_o is 7.9×10^{-9} emu, obtained by choosing an average period equal to the epoch interval, namely, 10 yrs.~~

According to the assumed distribution of conductivity $\sigma = \sigma_o \rho^{-\gamma}$, the value of γ in Eq. (38) implies that the conductivity at the core-mantle boundary is only 10.6 times that at the 1,000 km depth ~~($=3.39 \times 10^{-9}$ emu)~~; below this depth σ is essentially uniform. At lesser depths, one would hardly expect the secular field to be successfully employed in the computation of σ since the physical attenuations C_n are scarcely influenced by the outer 1/3 portion of the mantle. At the earth's surface typical values of σ are as follows: wet ground, 10^{-13} to 10^{-14} emu; dry ground, 10^{-15} to 10^{-16} emu; fresh water, 10^{-14} emu; sea water, 4×10^{-11} emu. Compatible with the results of Lahiri and Price (1939), it follows that σ must increase very steeply in the outer 1/3 portion of the mantle.

The tentative results (38) and (39) are considered here as only orders of magnitude; the precision has yet to be established. This will entail an investigation of the various factors influencing the critical values of γ and δ. Unfortunately, several of the computed ratios B_i/B_j, for which $i \neq j$, are incompatible with the ratios computed from Chapter III. These ratios are indicated by an asterisk in Appendix D. Some difficulty lies in the scanty data. Of particular trouble is the small dipole term which may be indicative of a weak θ-dependence (Observe that no difficulty exists for the ratio B_2/B_1 when (37) is employed.)

The final conclusions of this chapter will be contained in Part II of this report.

VI. Observatory Records

Further information concerning the nature of the electromagnetic waves passing through the mantle may be found from an examination of the magnetic observatory records. Vestine's maps of the secular variation fields represent 10 yr. averages centered at the various epochs. Since many observatory records show disturbances of much shorter duration, considerable activity is not represented in these maps. Figures 16 through 22 illustrate this point. The values of $\dot{H}$ (horizontal component) and $\dot{H}_r$ (= $-\dot{Z}$) were scaled from Vestine's graphs of the time variation of the earth's main field (ref. 4, pp. 151-249). The solid- and open-circles in Figs. 16, 18, 20, 22 indicate map values of $\dot{H}$ and $\dot{H}_r$, respectively . Evidently a rapidly moving ridge at the core would not be recorded on the maps.

The examples clearly show that no appreciable relative amplitude attenuation occurs for wave periods greater than three or four months.

All the stations represented by Vestine's data, 99 magnetic observatories, were examined for a possible phase relation between $\dot{H}_r$ and $\dot{H}$ components. Of the stations represented, 16 were deleted because of insufficient data (either the H- or Z- component was missing or the time interval covered was too short.) The remaining stations were catalogued according to the phase relation between the vertical and horizontal components: 23 stations were characterized strongly by a "180° phase difference"; $\dot{H}_r$ and $-\dot{H}$ increase and decrease together. Figures 16, 17 and 22 are typical examples. Twenty additional stations were counted as being typified by the 180° phase difference over a large portion of the range 1905 to 1945, but with exceptions. Figures 18 and 19 are examples of this latter class, although several of the observatory records counted here were not as consonant. Thirty-four stations were counted in which there was no consistent time relationship between $\dot{H}_r$ and $\dot{H}$. Only six

examples were counted in which $\dot{H}_r$ and $\dot{H}$ were strongly in phase. Figures 20 and 21 show one such station at Watheroo, Australia. The five remaining stations are Zaimishche-Kasan, Russia; Kotchíno, Russia; Coimbra, Portugal; San Juan, Puerto Rico; Tananarive, Madagascar Island. Eight typical examples for which there is no consistent phase relation are Chelyuskin, Siberia; Hongkong, China; Vienna, Austria; Nantes, France; San Fernando, Spain; Sitka, Alaska; Pilar, Argentina; Batavia, Java. Eight typical examples for which there is a 180° phase relation are Elisabethville, Belgian Congo; Yakutsk, Siberia; Toyohara, Japan; Tsingtao, China; Toungoo, Burma; Uccle(Brussels) Belgium; Meanook, Canada; Tuscon, Arizona.

The occurrence of this out-of-phase relation is sufficiently striking to warrant further investigation. Perhaps the effect is pure within the core, and is partially obscured at the earth's surface by a superposition of different sources together with the quasi-dispersive effect (Chapter III).

Appendix A

The following tables list the algebraic average of A_n^m and B_n^m for Vestine's $\dot{X}$ and $\dot{Y}$ analyses (cf. ref. 6, p. 42), hereafter referred to as A_n^m and B_n^m.

A_n^m

m	n	1912.5	1922.5	1932.5	1942.5
0	1	2470	2839	2298	919
0	2	-1385	-2061	-2815	-3574
0	3	1695	1995	1258	533
0	4	1005	1054	1935	1825
0	5	-2384	-1946	1031	-1146
0	6	684	763	400	1395
1	1	97.5	367.5	134.5	157.5
1	2	-258.5	130.5	264.5	22.5
1	3	-1652	-2228	-2195	-2195
1	4	1650	1270	995.5	612
1	5	-1105	-939	-761.5	274.5
1	6	908	151.5	814	-99.0
2	2	4758	3302	1965	489.5
2	3	-408	-588	213	1000
2	4	-1070	-735	-1067	-386.5
2	5	-2004	-1479	-1492	-777
2	6	464	454	1146	800
3	3	4028	2225	944.5	24
3	4	-307	-262	674	1156
3	5	-1189	-589	-318	- 95.5
3	6	-1114	-1026	-671.5	-433
4	4	1970	1400	1343	1053
4	5	-1751	-1045	-1089	-335
4	6	587.5	569	757.5	578.5
5	5	-2551	-1045	-937	-691.5
5	6	-128	-692	-529.5	-816
6	6	-1498	-1063	-1078	-104

B_n^m

m	n	1912.5	1922.5	1932.5	1942.5
1	1	-688.5	-727.5	-465.5	133.5
1	2	-1858	-2810	-3523	-3943
1	3	-1808	-1473	-1557	-170.5
1	4	-1540	-872.5	-1721	-1256
1	5	3561	3289	3124	2349
1	6	73.5	-1060	-1060	-1143
2	2	-3418	-3429	-2745	-2831
2	3	924.5	901.5	1053	1241
2	4	-2302	-2219	-2277	-2358
2	5	442.5	587	686	1005
2	6	1412	856.5	71.5	415
3	3	-3316	-3330	-3835	-3134
3	4	395.5	1351	1259	1188
3	5	376.5	-391.5	-249	-436
3	6	385.5	314.5	226	166
4	4	-836	-1019	-1374	-891.5
4	5	-199.5	- 8.5	-38	-13.5
4	6	1229	721	624.5	17.5
5	5	1316	702	1384	1491
5	6	-1189	-897	-482	-473
6	6	472	1241	933	736

Appendix B

The following table lists the time average (for the four epochs) of $|A_n^m|$, $|B_n^m|$ and $\frac{1}{2}(|A_n^m| + |B_n^m|)$. Also, the latter quantity is averaged with respect to m = 0,1,...n.

m	n	$\|A_n^m\|_t$	$\|B_n^m\|_t$	$\frac{1}{2}(\|A_n^m\|_t + \|B_n^m\|_t)$
0	1	2132		2132
0	2	2459		2459
0	3	1370		1370
0	4	1455		1455
0	5	1627		1627
0	6	810.5		810.5
1	1	189.2	503.7	346.5
1	2	169.0	3033	1601
1	3	2067	1252	1660
1	4	1132	1347	1240
1	5	769.7	3080	1925
1	6	493.1	834	663.6
2	2	2628	3105	2867
2	3	552.4	1030	791.2
2	4	814.6	2289	1552
2	5	1438	680	1059
2	6	715.9	688.8	702.3
3	3	1805	3403	2604
3	4	599.7	1048	823.9
3	5	547.9	363.2	455.6
3	6	811	273	542
4	4	1441	1030	1236
4	5	1055	64.9	559.9
4	6	623.1	647.9	635.5
5	5	1306	1223	1265
5	6	541.4	760.1	650.7
6	6	935.7	845.5	890.6

n	average, m=0,1,...n	n	average, m=0,1,...n
1	1739	4	1261
2	2309	5	1148
3	1606	6	699.3

Appendix C

m	n	$\sum_{1912.5}^{1942.5} \lvert A_n^m \rvert^2$	$\sum_{1912.5}^{1942.5} \lvert B_n^m \rvert^2$
0	1	**20,286,186**	
0	2	**26,863,647**	
0	3	8,719,703	
0	4	9,195,791	
0	5	11,846,649	
0	6	3,156,050	
1	1	187,459	1,237,801
1	2	154,319	39,303,519
1	3	17,323,064	7,888,883
1	4	5,701,345	7,669,438
1	5	2,755,935	38,763,097
1	6	1,519,813	3,557,992
2	2	37,632,579	38,980,760
2	3	1,558,577	4,316,292
2	4	2,972,996	20,968,058
2	5	9,031,246	2,019,992
2	6	2,373,582	2,903,262
3	3	22,068,065	46,606,773
3	4	1,953,505	4,974,249
3	5	1,870,886	547,121
3	6	2,931,048	326,153
4	4	8,750,393	4,419,905
4	5	5,456,172	41,499
4	6	1,577,386	2,419,360
5	5	8,955,767	6,360,323
5	6	1,441,474	2,673,194
6	6	4,546,873	3,175,050

Appendix D

Table of B_i/B_j

i/j	Eq. 34 Table 4	Eq. 34 Table 5	Eq. 36 $\alpha=5^o$ Table 4	Eq. 36 $\alpha=5^o$ Table 5	Eq. 36 $\alpha=15^o$ Table 4	Eq. 36 $\alpha=15^o$ Table 5	Eq. 37 $\alpha=20^o$ Table 4	Eq. 37 $\alpha=20^o$ Table 5	Eq. 37 Δ_{ij}
6/1	.382	.422	.169	.187	.209	.231	.116	.128	.456
5/1	.696	.608	.335	.292	.387	.338	.161	.141	.365
4/1	.693	.832	.369	.443	.405	.487	.174	.209	.395
3/1	1.054*	1.116*	.643	.681	.677	.717	.327	.346	.462
2/1	1.572*	1.504*	1.134*	1.085*	1.182*	1.131*	.730	.699	.606
6/2	.243	.280	.146	.169	.177	.204	.124	.143	.589
5/2	.443	.404	.289	.264	.328	.299	.221	.201	.602
4/2	.441	.553	.319	.400	.343	.430	.238*	.299	.651
3/2	.671	.742	.555	.614	.573	.634	.448*	.496*	.761
6/3	.363	.378	.263	.274	.309	.322	.277	.289	.774
5/3	.661	.544	.521	.429	.572	.471	.493	.406	.790
4/3	.657	.745	.574	.651	.599	.679	.532*	.603	.855
6/4	.552	.507	.459	.421	.516	.474	.521	.479	.905
5/4	1.005*	.730	.907	.658	.956	.694	.928	.674	.924
6/5	.549	.694	.506*	.640	.539*	.682	.562	.711	.979

Note: All the columns(except the last column, Δ_{ij}) list the ratio B_i/B_j computed from the appropriate Equation and Table. The asterisked ratios are incompatible with those computed in Chapter III.

References

1. McDonald, K.L.; Technical Report No. 15, Earth's magnetism and magnetohydrodynamics, contract Nonr 1288(00), Office of Naval Research. See also J. Geophys. Res., 60, 1955.
2. Lahiri, B.N., and A.T. Price (1939); Phil.Trans. R. Soc., A, 237, 509.
3. Elsasser, W.M. (1950); Rev. Mod. Phys., 22, 1.
4. Elsasser, W.M. (1954); Physical Review, 95, 1.
5. Vestine, E.H., L. Laporte, I. Lange, C. Cooper, and W.C. Hendrix (1947); Carnegie Inst. Wash. Pub. No. 578.
6. Vestine, E.H., L. Laporte, I. Lange, and W.E. Scott (1947); Carnegie Inst. Wash. Pub. No. 580.
7. Jahnke, E., and F. Emde (1945); Tables of functions, Dover Publications, Inc., New York.
8. Dwight, H.B. (1941); Mathematical Tables, McGraw-Hill Book Co., Inc. New York and London.
9. Whittaker, E.T., and G.N. Watson (1950); A Course of Modern Analysis, Cambridge Univ. Press.
10. Stratton, J.A. (1941); Electromagnetic Theory, McGraw-Hill Book Company, Inc, New York and London.
11. Copson, E.T. (1935); Theory of Functions of a Complex Variable, Oxford Univ. Press.

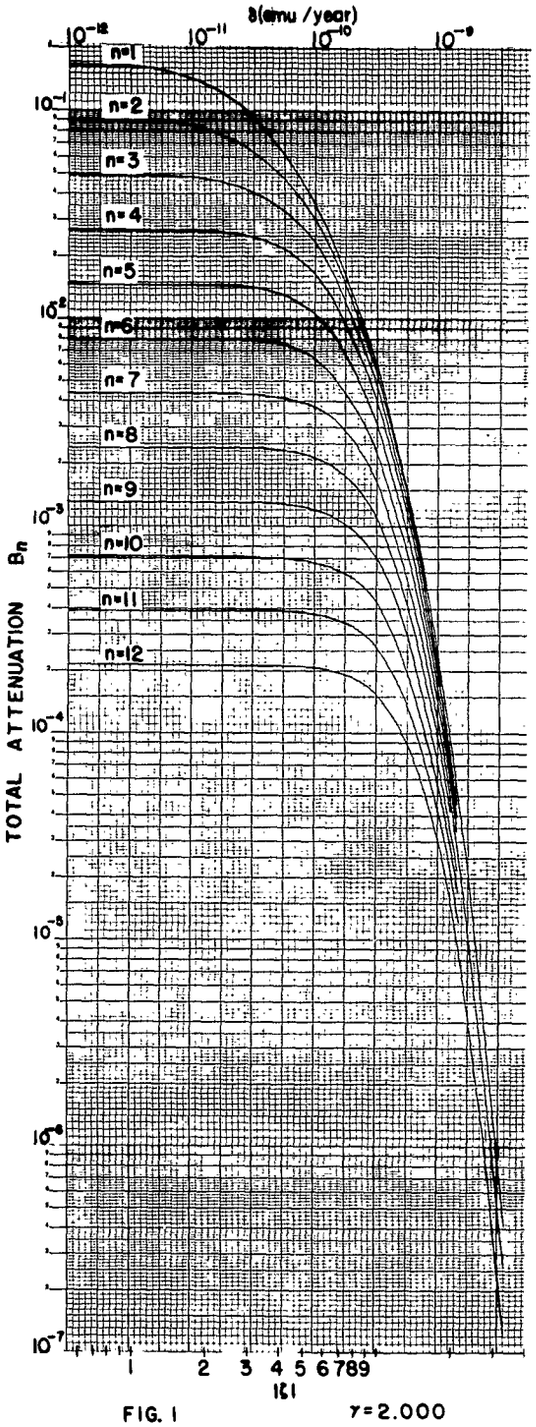

FIG. 1 γ=2.000

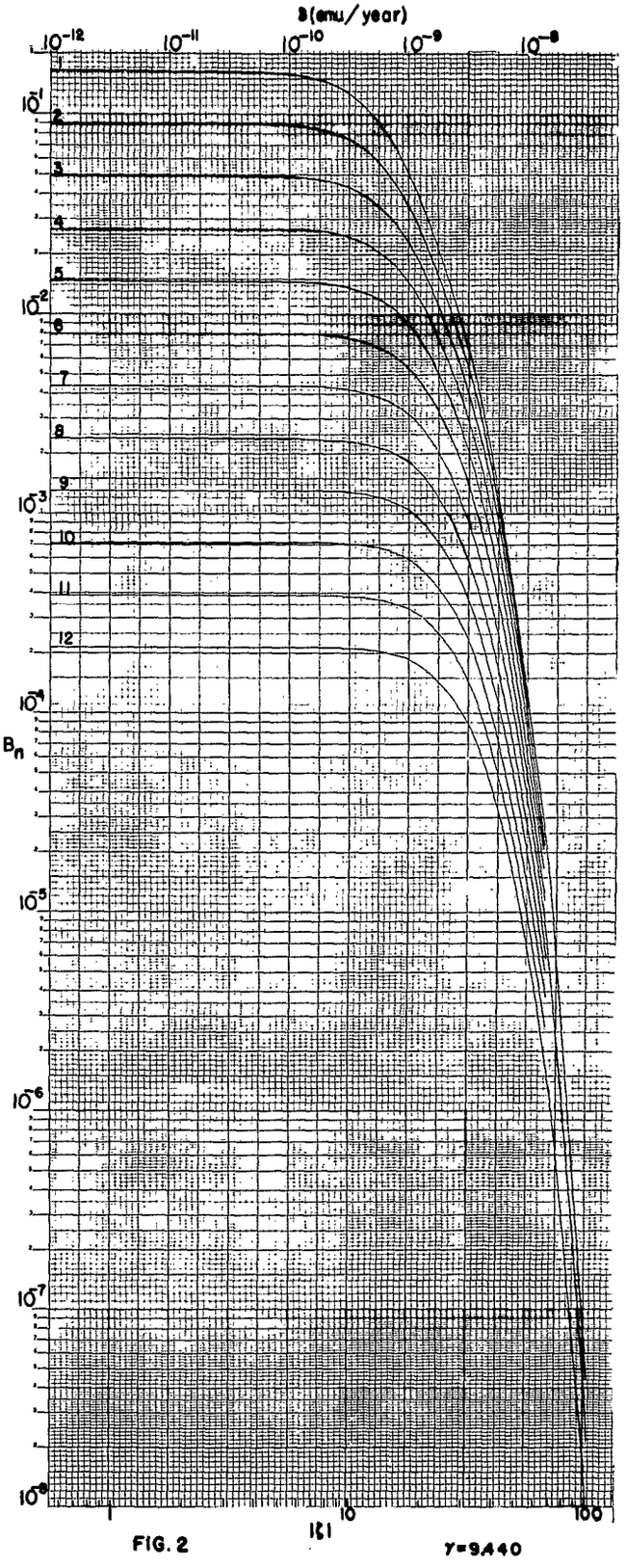

FIG. 2 γ=9.440

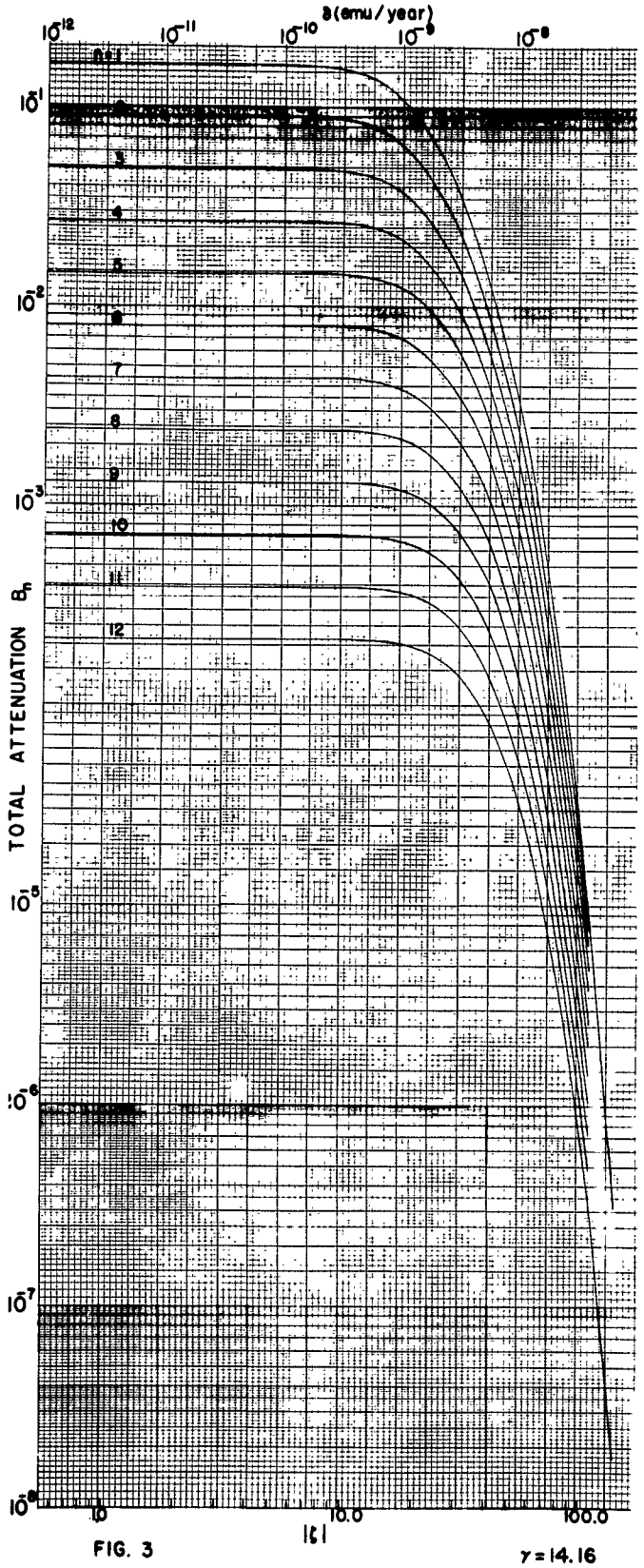

FIG. 3

$\gamma = 14.16$

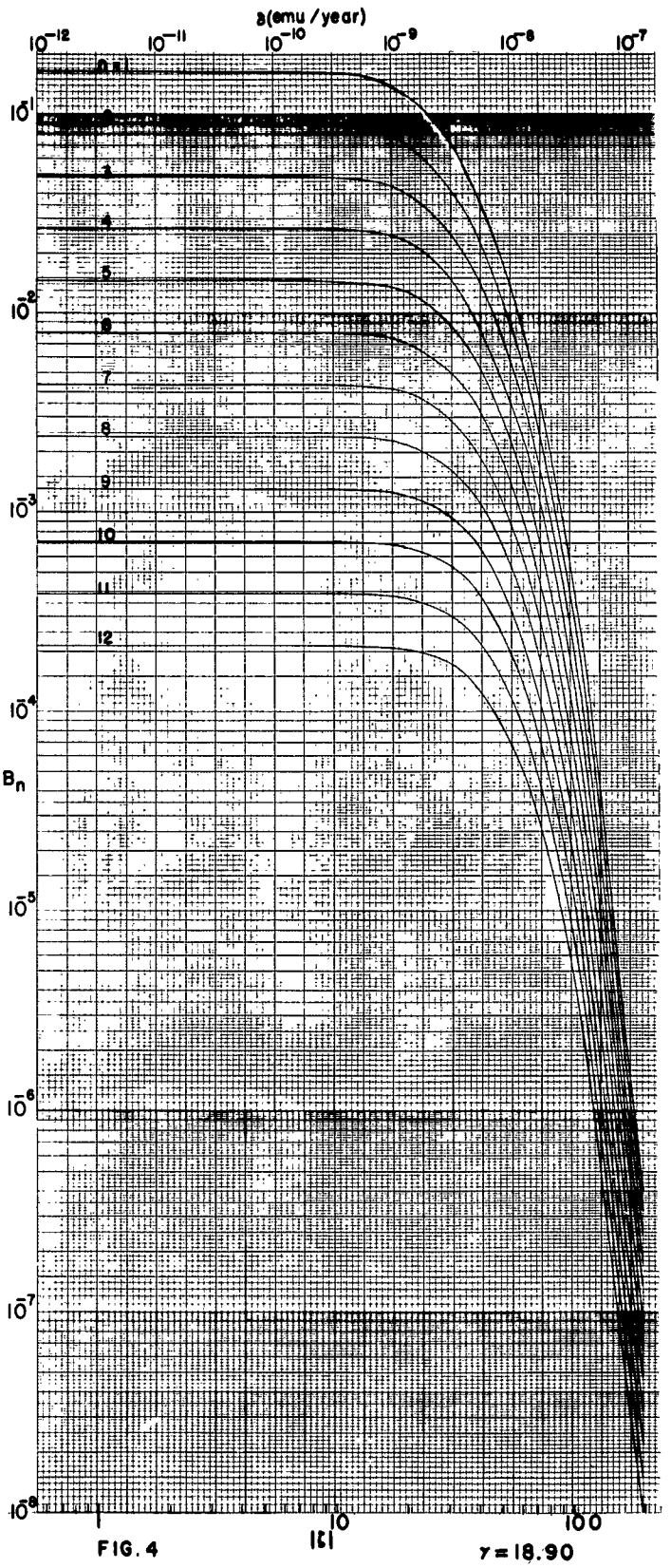

FIG. 4

$\gamma = 18.90$

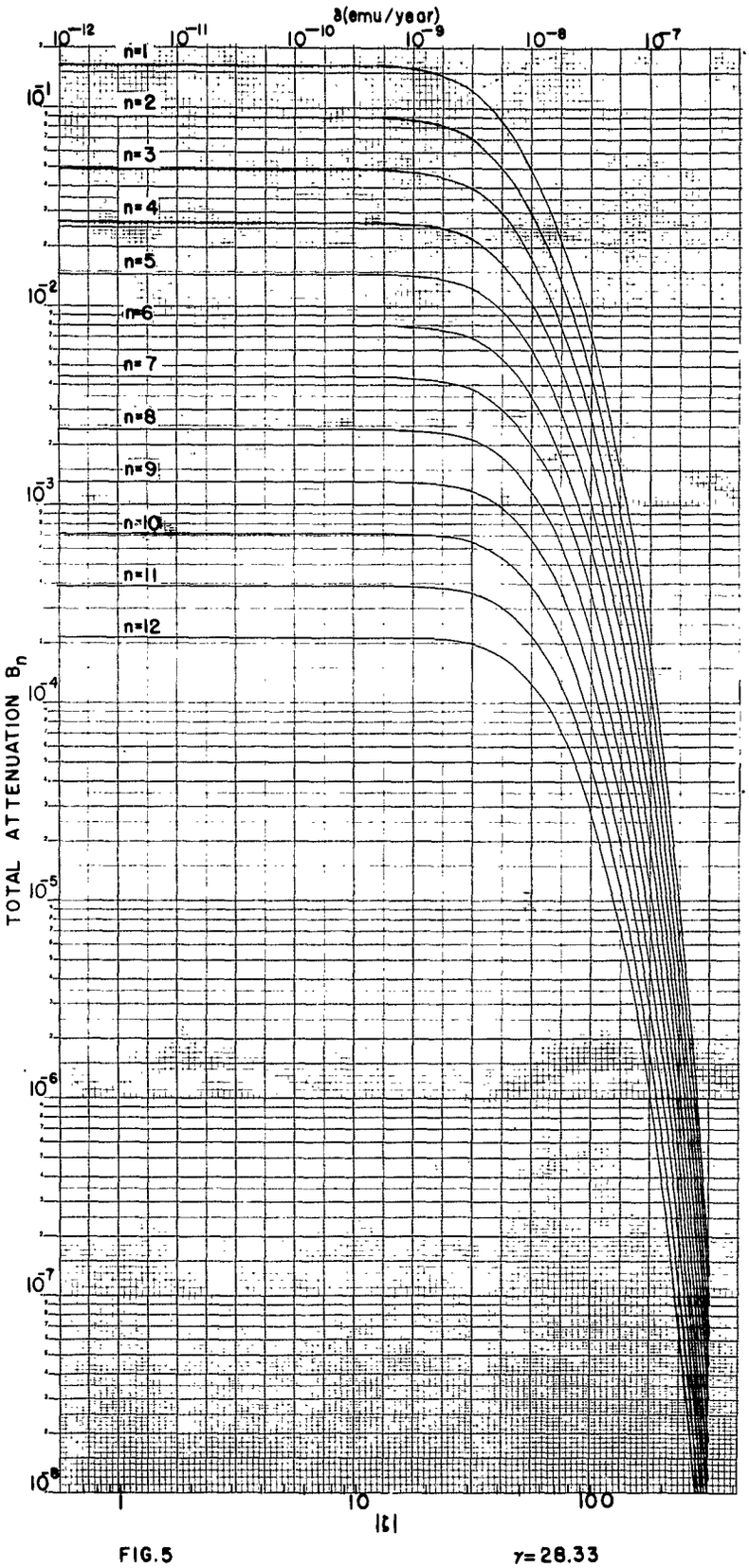

FIG.5

$\gamma = 28.33$

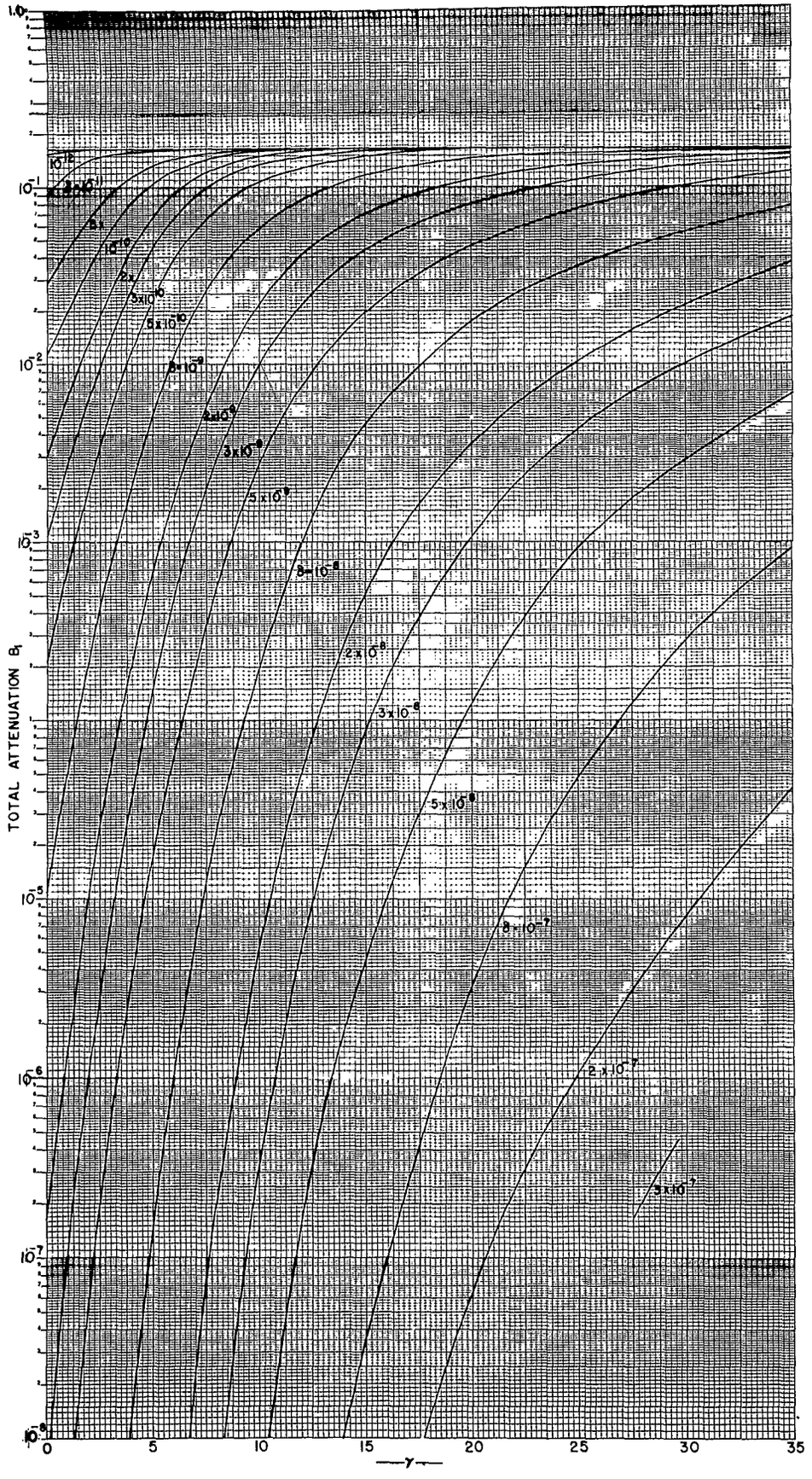
TOTAL ATTENUATION B_t
1.0
10^{-1}
10^{-2}
10^{-3}
10^{-5}
10^{-6}
10^{-7}
10^{-8}
10^{-15}
2×10^{-11}
10^{-10}
5×10^{-10}
8×10^{-10}
2×10^{-9}
3×10^{-9}
5×10^{-9}
8×10^{-8}
2×10^{-8}
3×10^{-8}
5×10^{-8}
8×10^{-7}
2×10^{-7}
3×10^{-7}
0
5
10
15
20
25
30
35
γ

Fig. 6

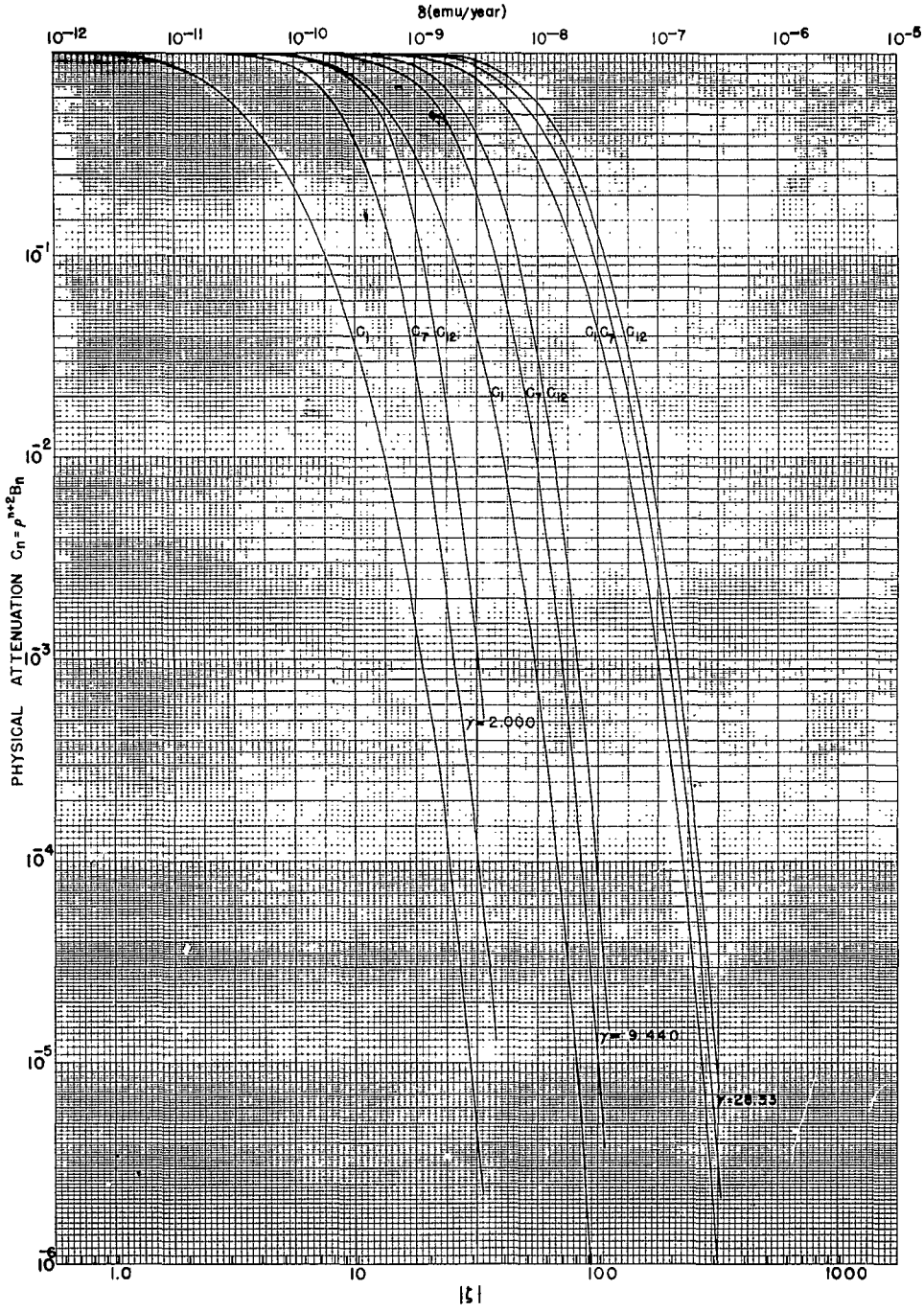
δ(emu/year)
10⁻¹²
10⁻¹¹
10⁻¹⁰
10⁻⁹
10⁻⁸
10⁻⁷
10⁻⁶
10⁻⁵
PHYSICAL ATTENUATION $C_n = \rho^{n+2} B_n$
10⁻¹
10⁻²
10⁻³
10⁻⁴
10⁻⁵
10⁻⁶
C₁ C₇ C₁₂
C₁ C₇ C₁₂
C₁ C₇ C₁₂
γ=2.000
γ=9.440
γ=28.33
1.0
10
100
1000
121

Fig. 7

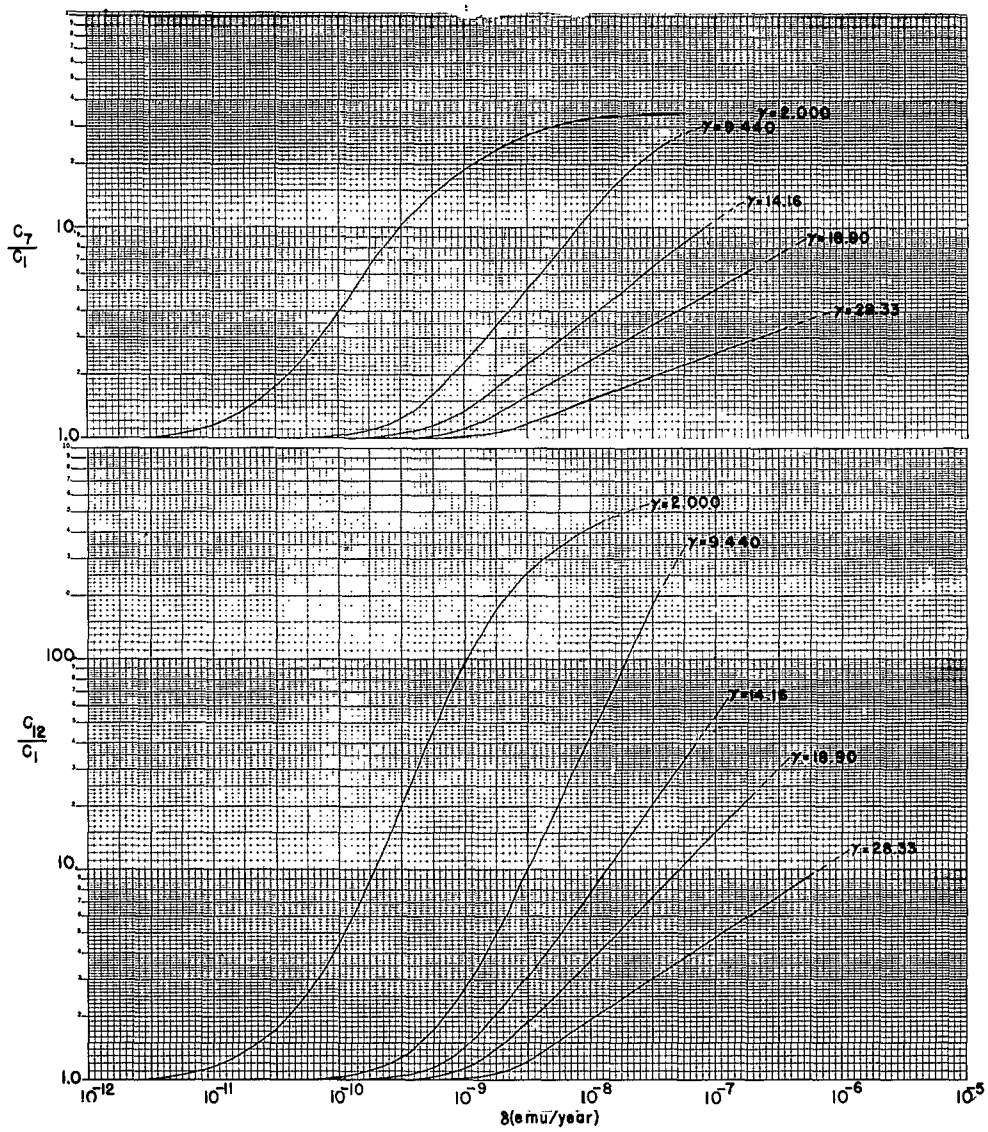

FIG. 8. RELATIVE PHYSICAL ATTENUATION

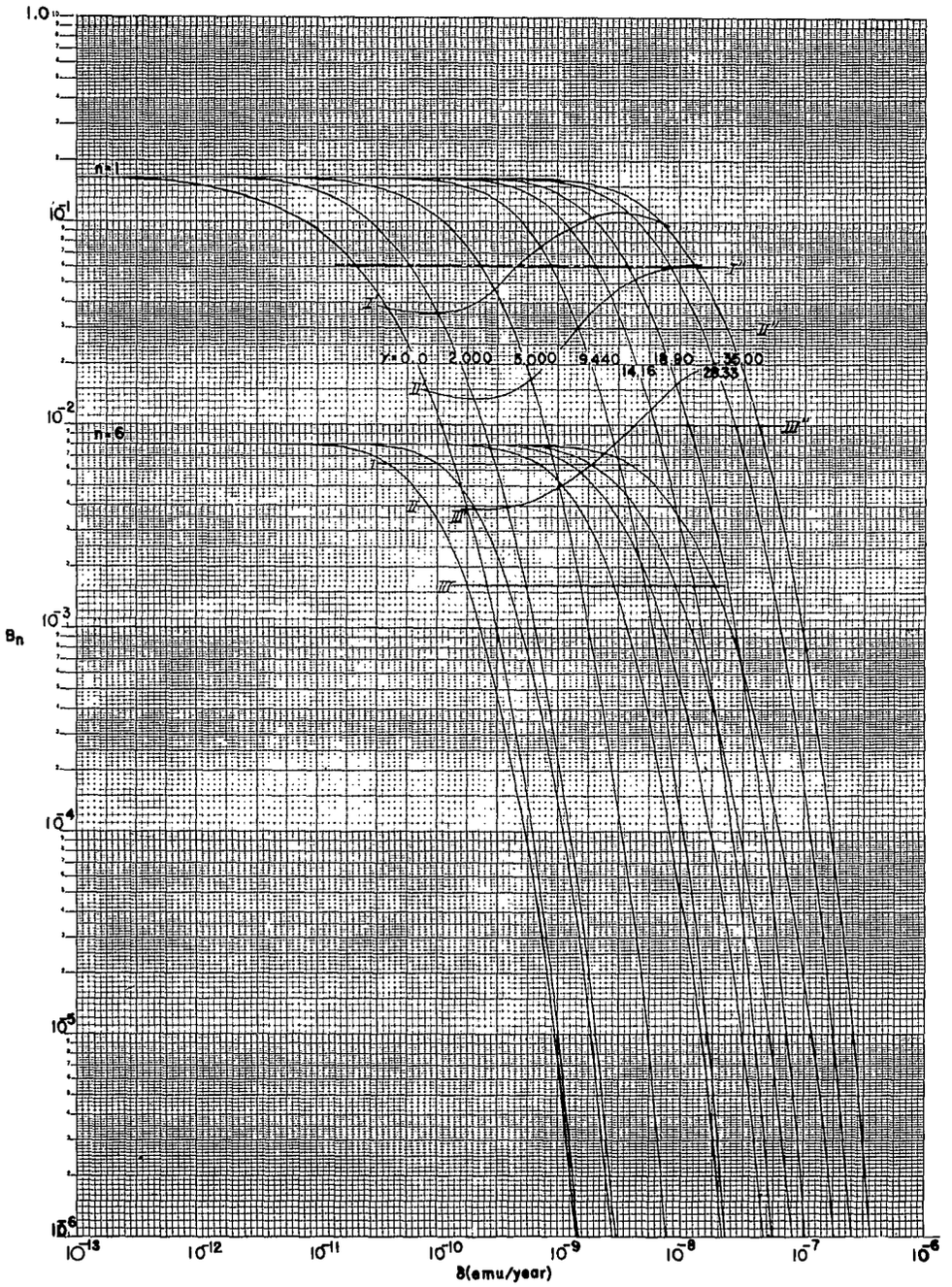
1.0
n=1
10^{-1}
10^{-2}
n=6
10^{-3}
10^{-4}
10^{-5}
10^{-6}
B_n
γ=0.0
2.000
5.000
9.440
14.16
18.90
23.33
35.00
I
I'
I''
II
II'
II''
III
III'
III''
10^{-13}
10^{-12}
10^{-11}
10^{-10}
10^{-9}
10^{-8}
10^{-7}
10^{-6}
β(emu/year)

FIG. 9

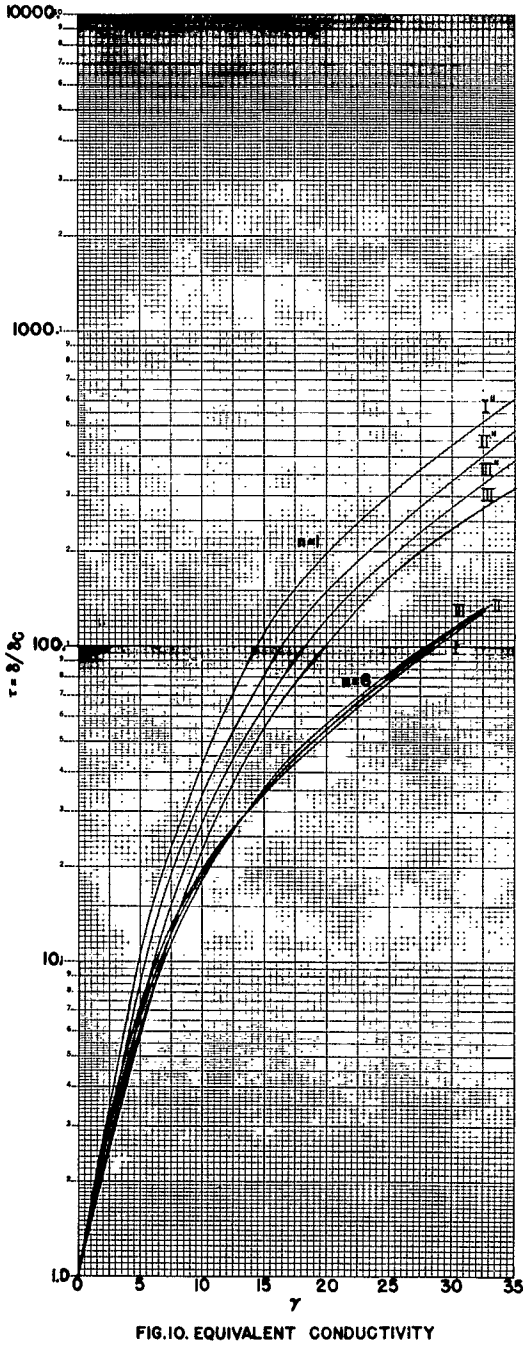

FIG. 10. EQUIVALENT CONDUCTIVITY

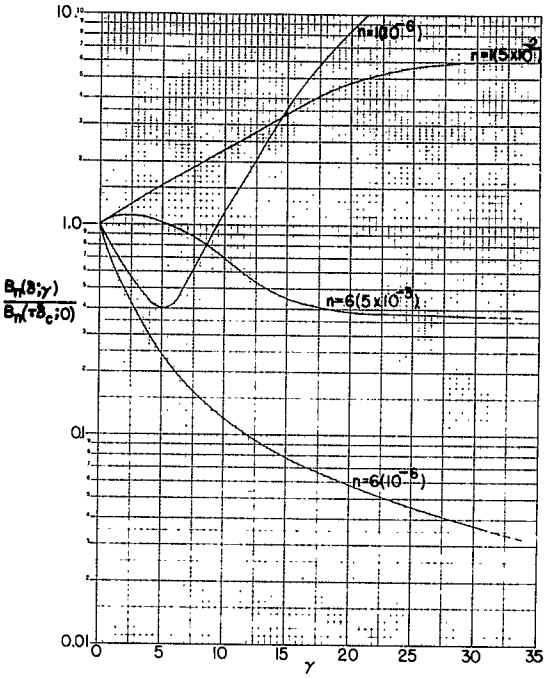

FIG. 11a

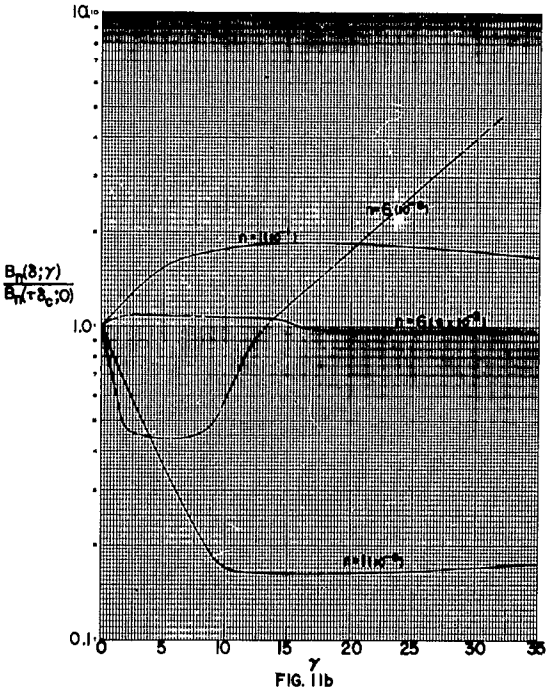

FIG. 11b

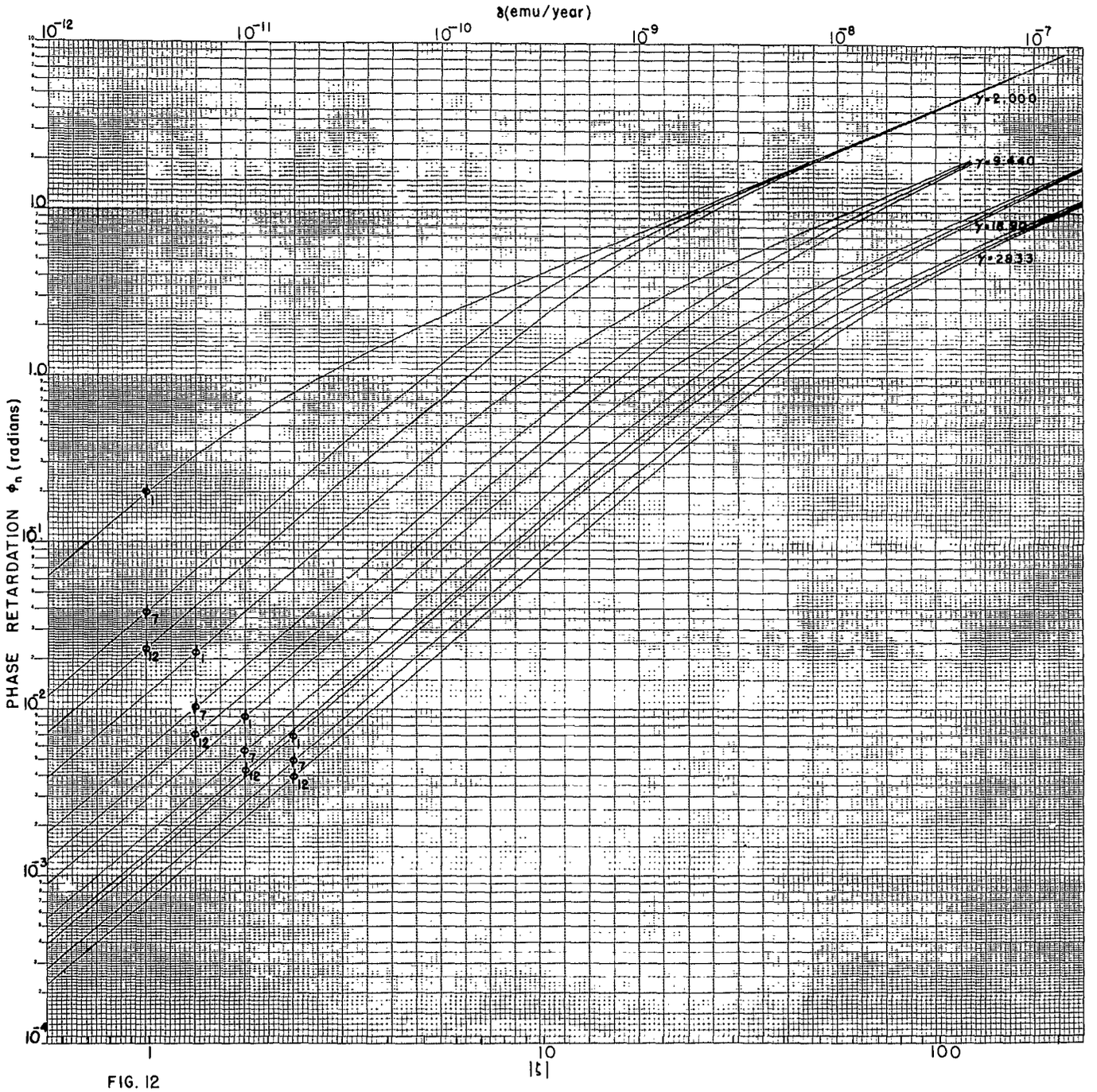
δ(emu/year)
10^{-12}
10^{-11}
10^{-10}
10^{-9}
10^{-8}
10^{-7}
γ=2.000
γ=9.440
γ=18.88
γ=28.33
PHASE RETARDATION ϕ_n (radians)
10
1.0
10^{-1}
10^{-2}
10^{-3}
10^{-4}
ϕ_1
ϕ_7
ϕ_{12}
1
10
100
|ξ|

FIG. 12

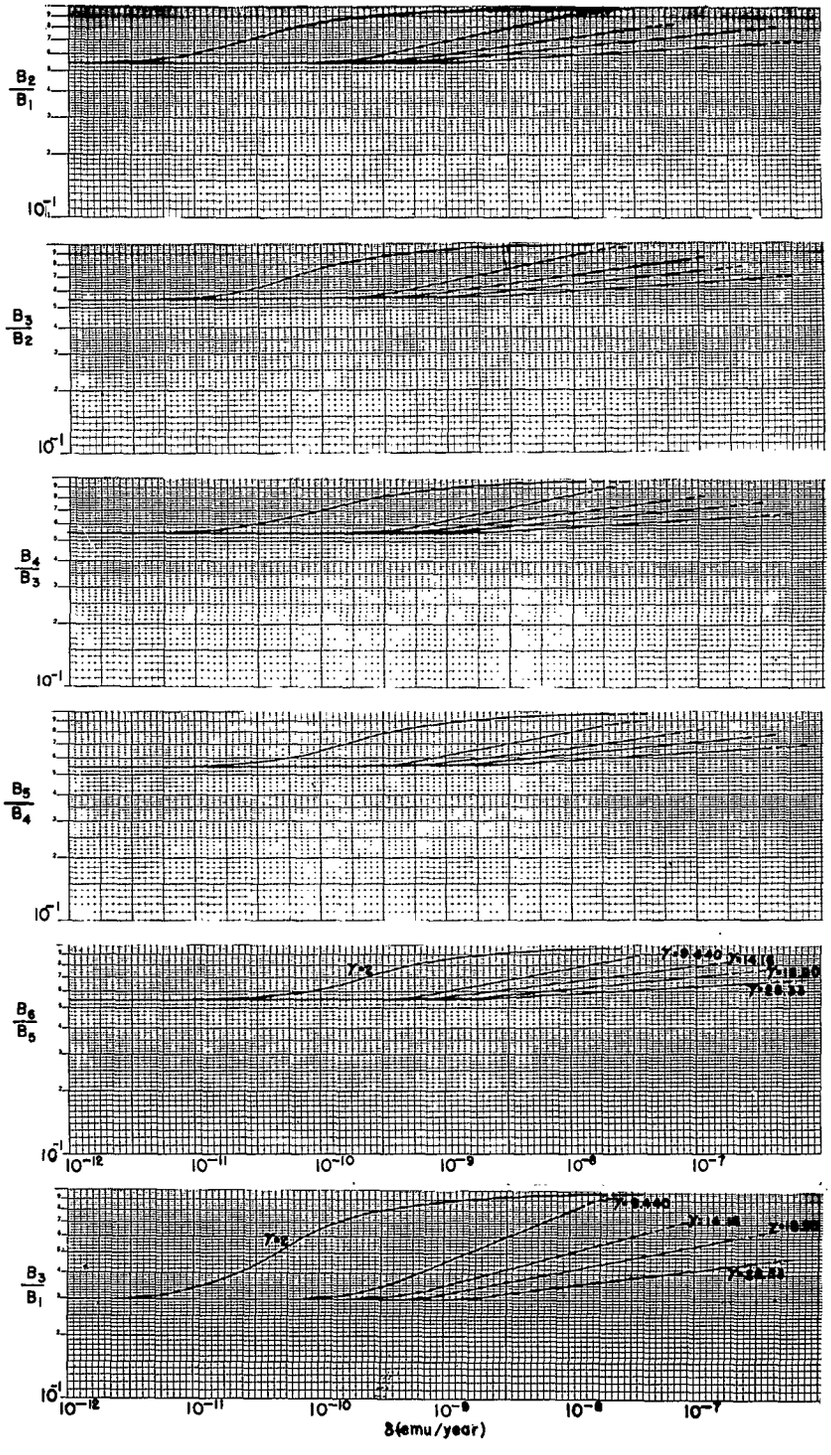
$\frac{B_2}{B_1}$
10^{-1}
$\frac{B_3}{B_2}$
10^{-1}
$\frac{B_4}{B_3}$
10^{-1}
$\frac{B_5}{B_4}$
10^{-1}
$\frac{B_6}{B_5}$
10^{-1}
10^{-12}
10^{-11}
10^{-10}
10^{-9}
10^{-8}
10^{-7}
$\frac{B_3}{B_1}$
10^{-1}
10^{-12}
10^{-11}
10^{-10}
10^{-9}
10^{-8}
10^{-7}
δ(emu/year)

FIG.13

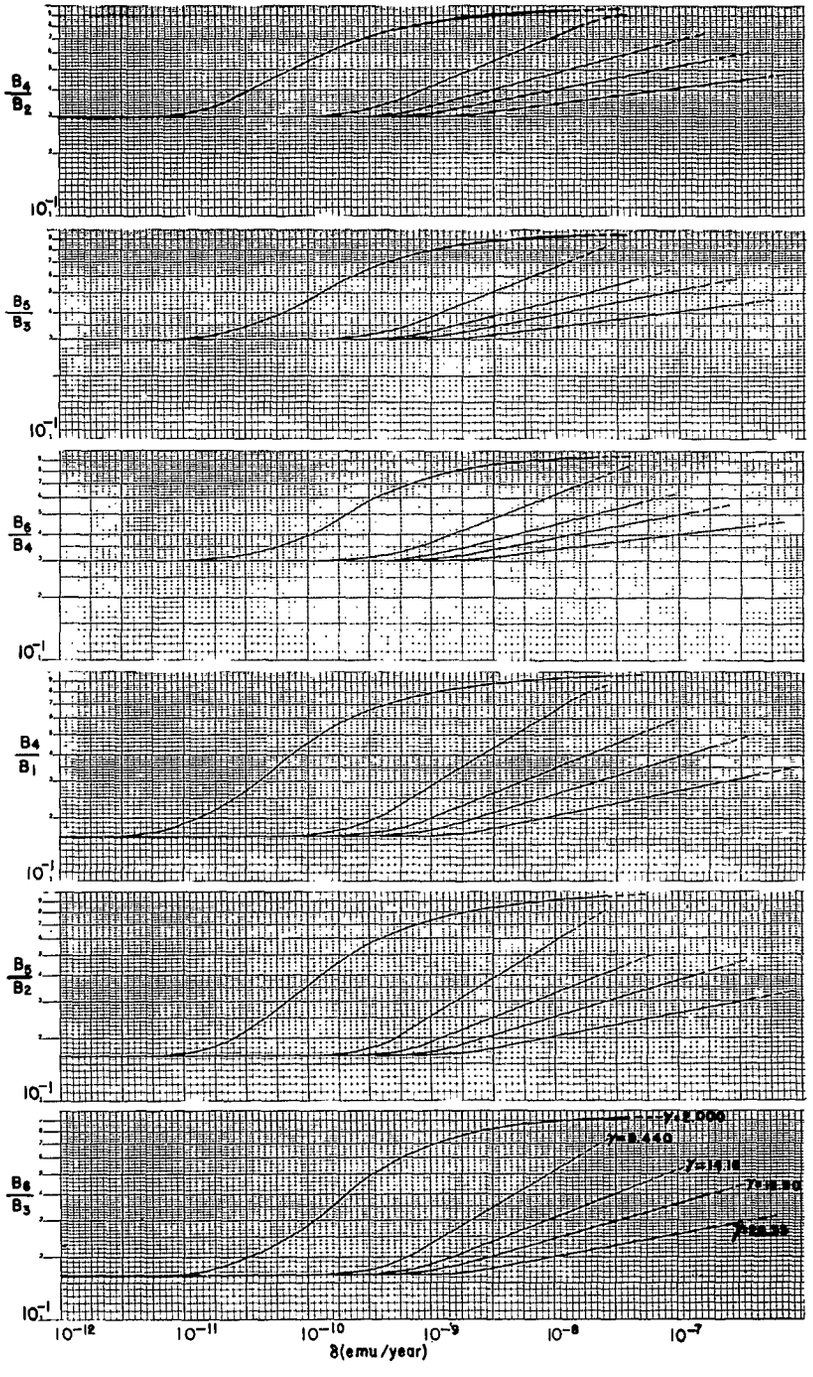
$\frac{B_4}{B_2}$
$\frac{B_5}{B_3}$
$\frac{B_6}{B_4}$
$\frac{B_4}{B_1}$
$\frac{B_5}{B_2}$
$\frac{B_6}{B_3}$
10^{-1}
10^{-12}
10^{-11}
10^{-10}
10^{-9}
10^{-8}
10^{-7}
δ(emu/year)
γ=8.440
γ=14.18

FIG. 14

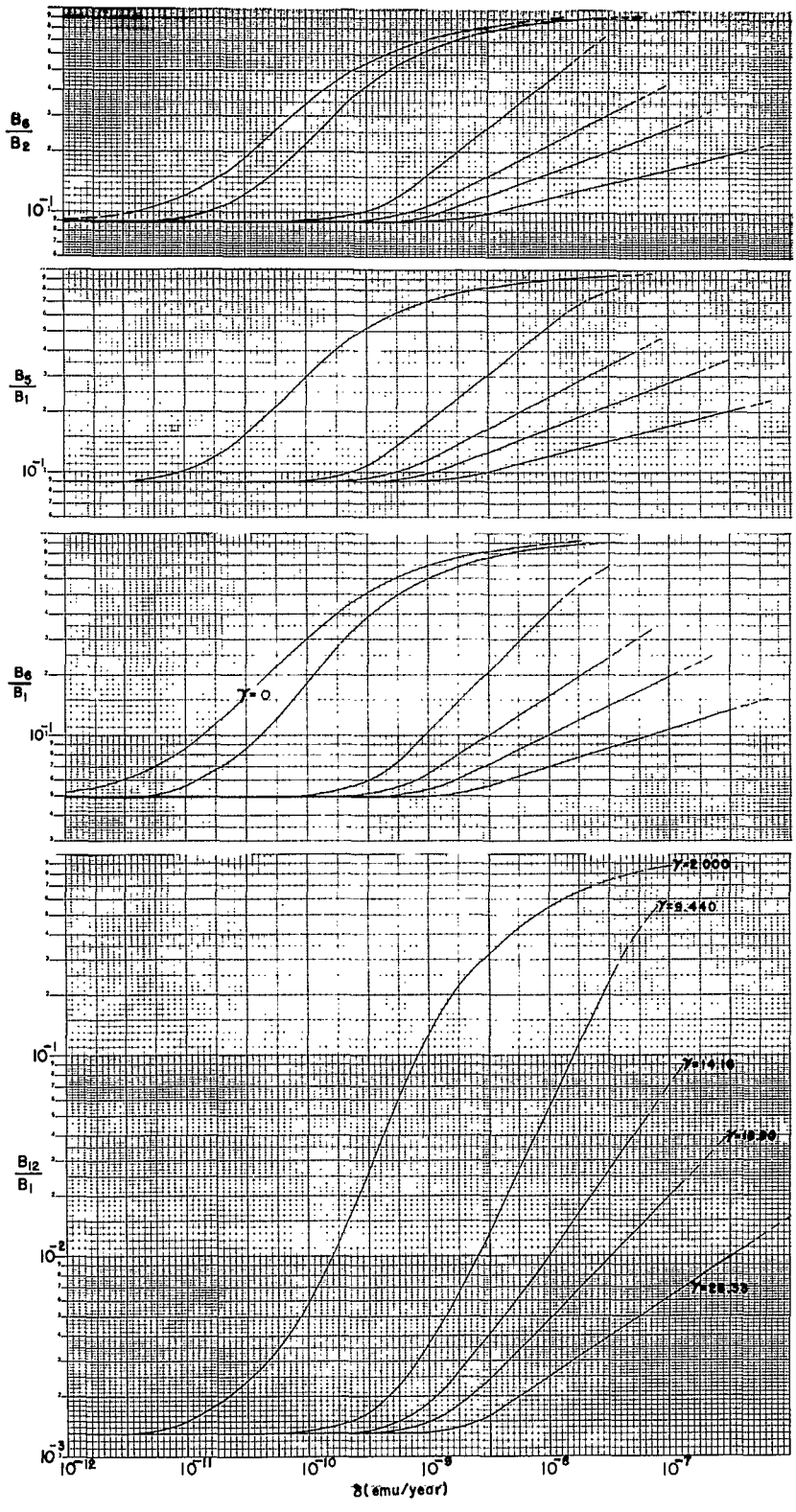
$\frac{B_6}{B_2}$
10^{-1}
$\frac{B_5}{B_1}$
10^{-1}
$\frac{B_6}{B_1}$
10^{-1}
γ = 0
γ = 2.000
γ = 9.440
γ = 14.16
γ = 18.88
γ = 28.32
$\frac{B_{12}}{B_1}$
10^{-1}
10^{-2}
10^{-3}
10^{-12}
10^{-11}
10^{-10}
10^{-9}
10^{-8}
10^{-7}
δ(emu/year)

FIG. 15

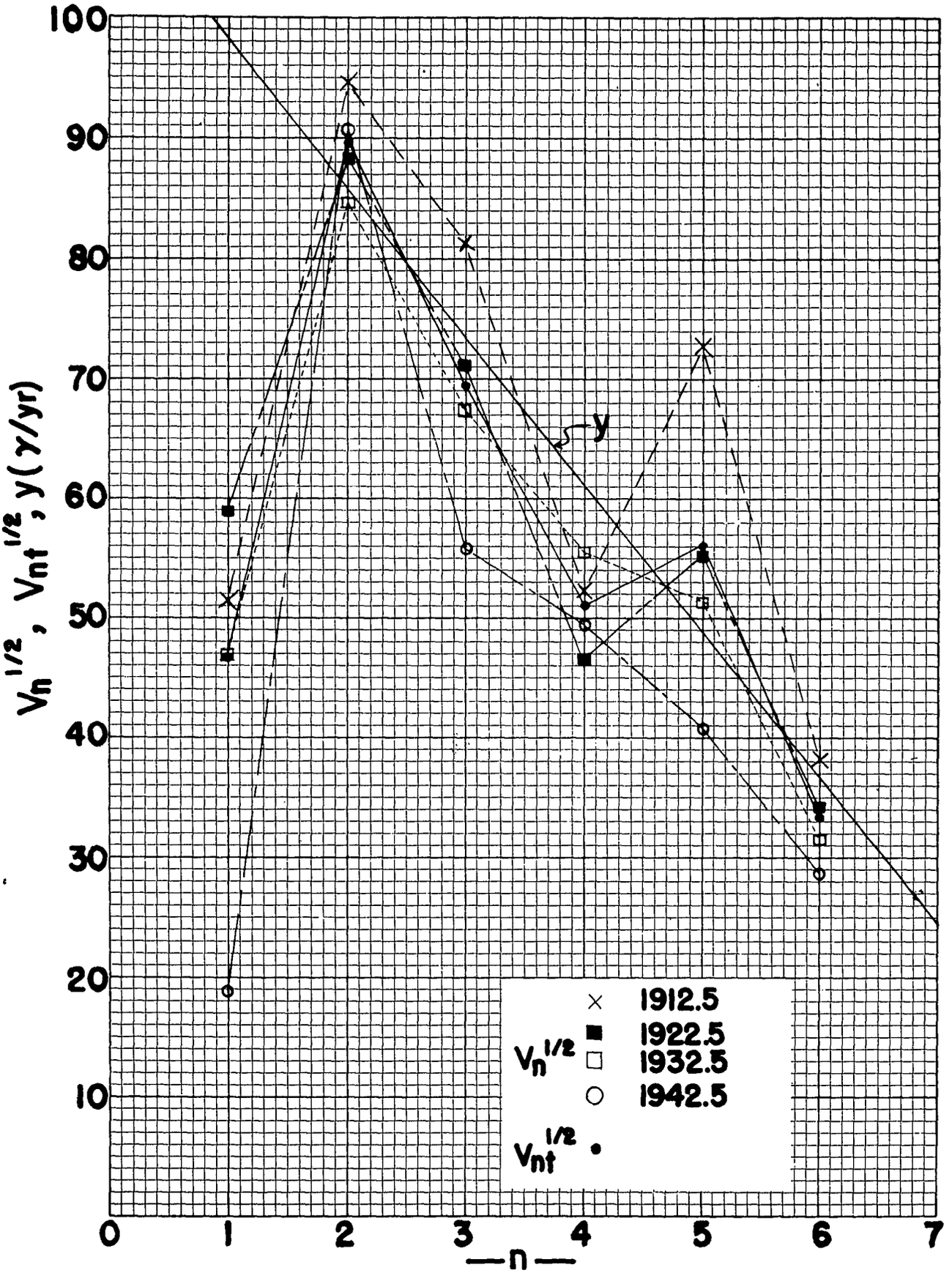
100
90
80
70
60
50
40
30
20
10
0
1
2
3
4
5
6
7
—n—
$V_n^{1/2}$, $V_{nt}^{1/2}$; y(γ/yr)
y
1912.5
1922.5
1932.5
1942.5
$V_n^{1/2}$
$V_{nt}^{1/2}$

FIG.15a.

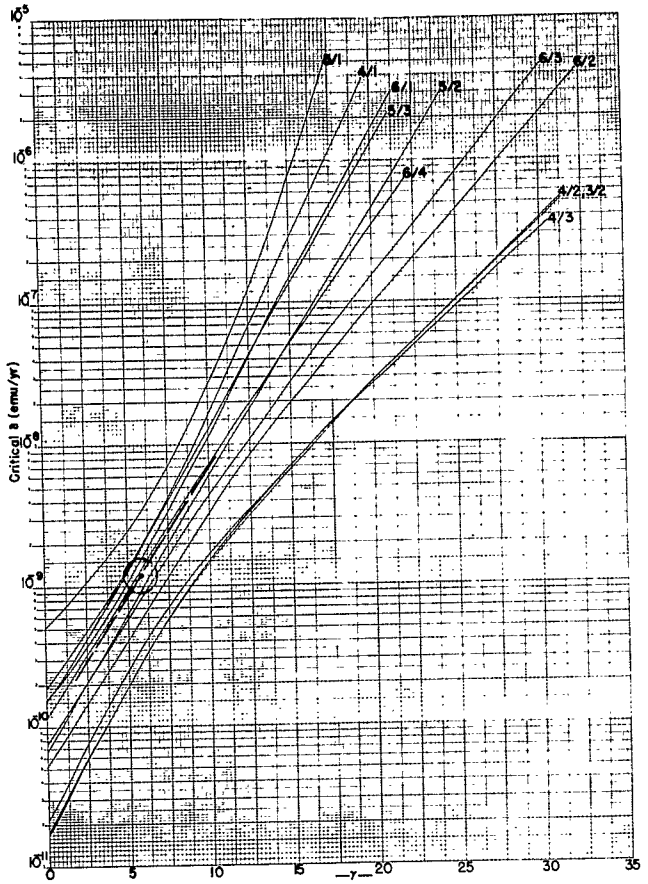

FIG.15b, B_i/B_j Computed from Eq. 34, Table 4.

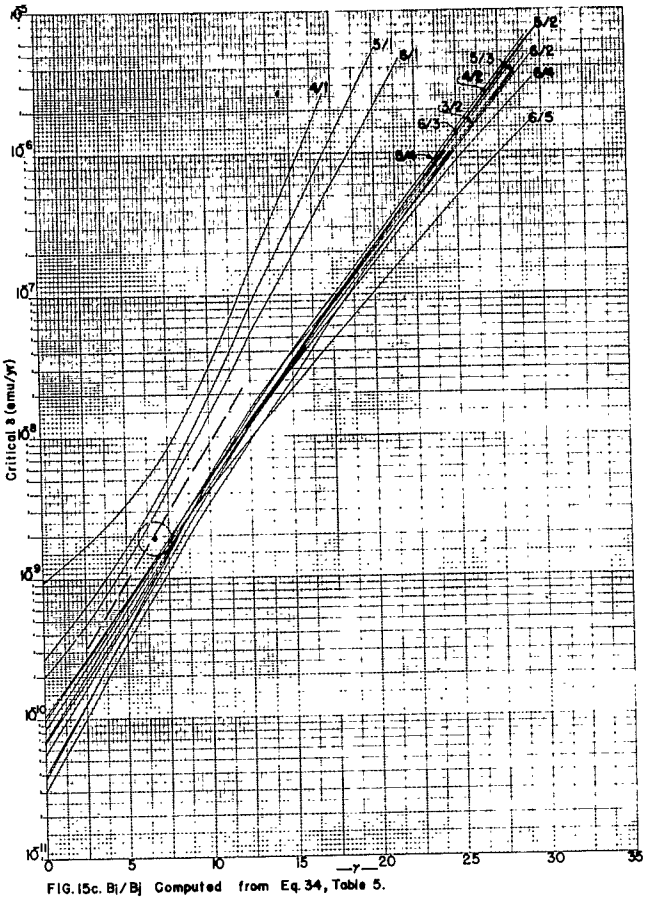

FIG. 15c. B_i/B_j Computed from Eq. 34, Table 5.

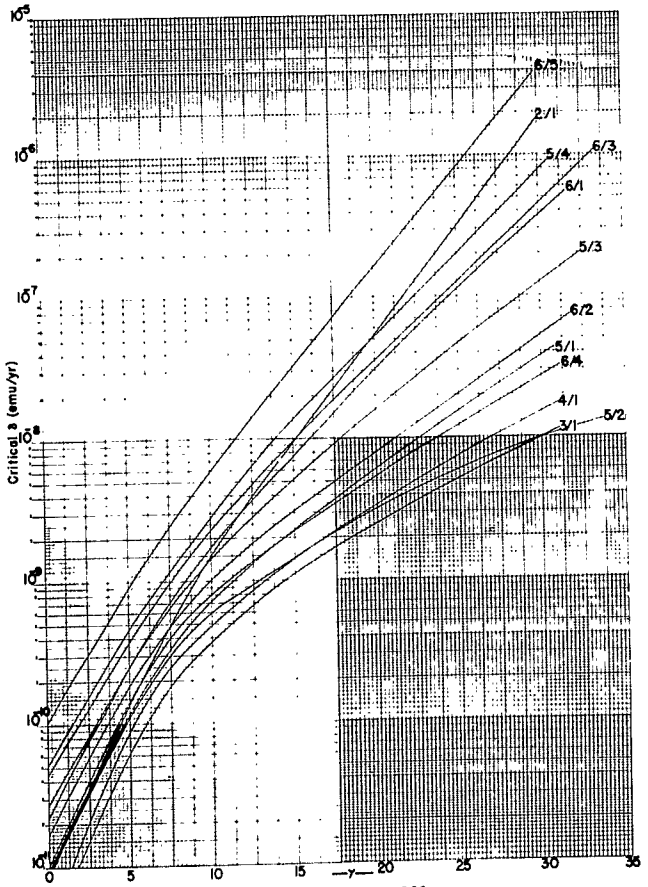

FIG. 15d, B_i/B_j Computed from Eq. 37, Table 5, $\alpha = 20°$.

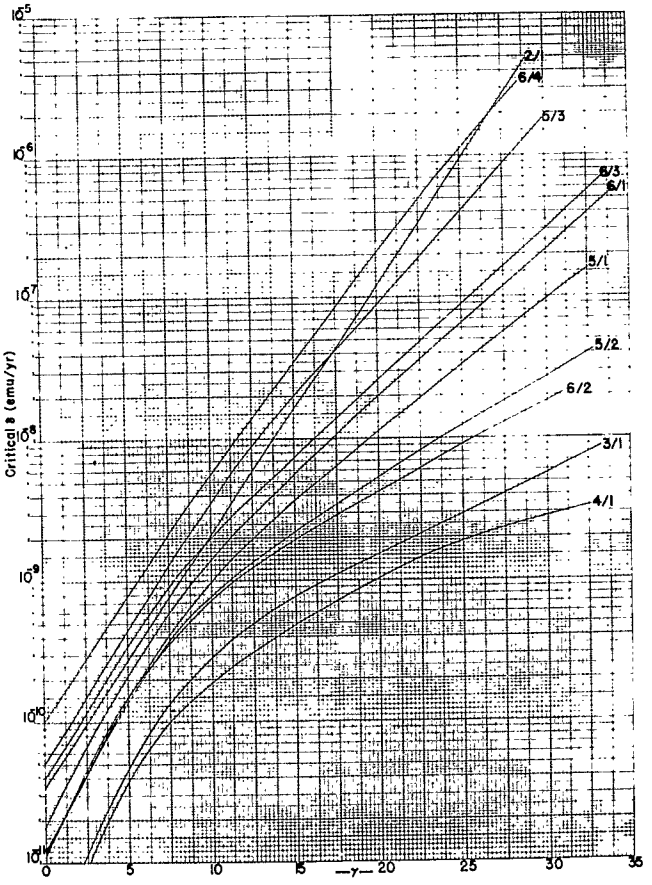

FIG. 15e, B_i/B_j Computed from Eq. 37, Table 4, $\alpha = 20°$.

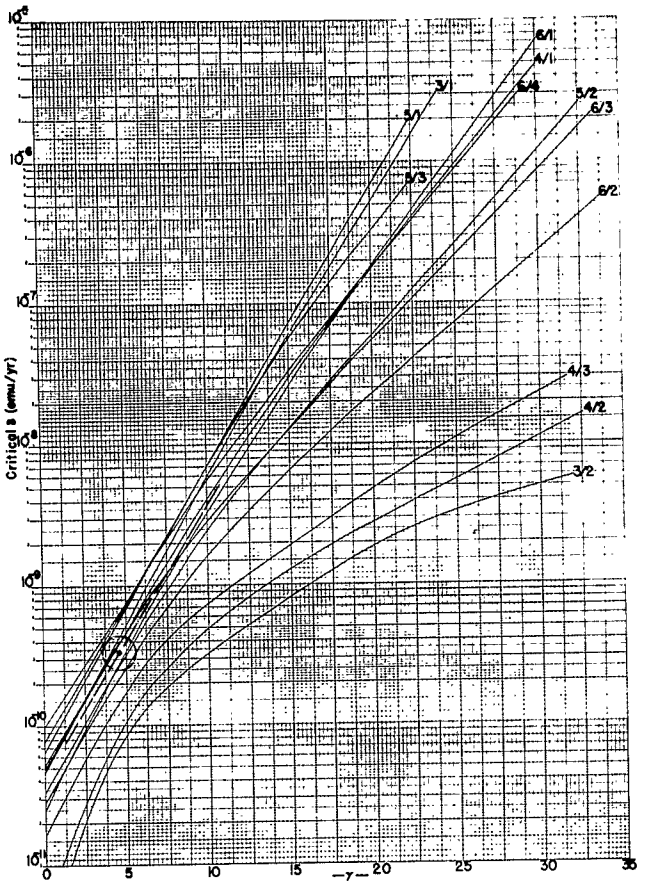

FIG. 15f, B_i/B_j Computed from Eq. 36, Table 4, $\alpha = 15°$.

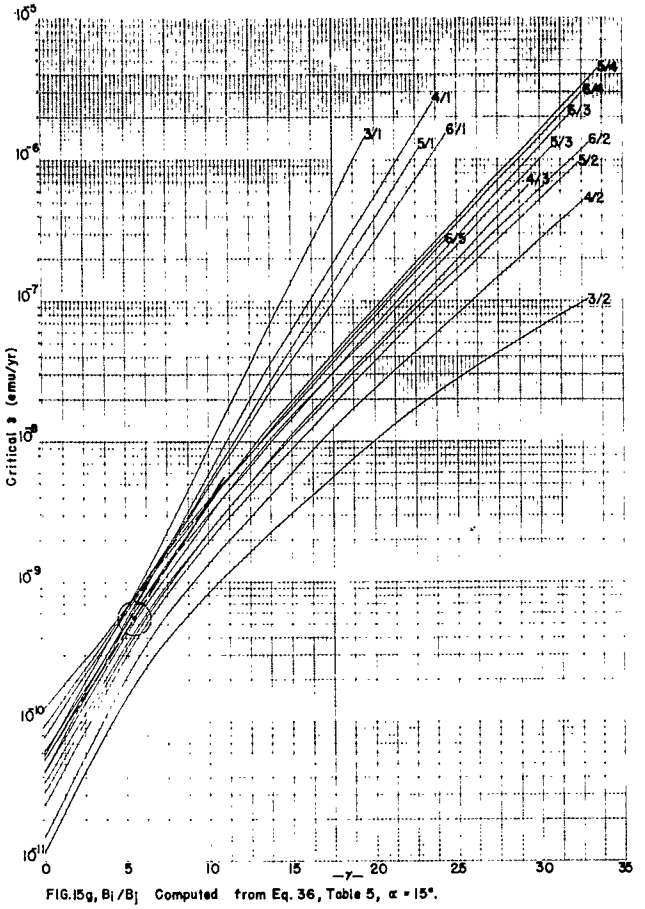

FIG. 15g, B_i/B_j Computed from Eq. 36, Table 5, $\alpha = 15°$.

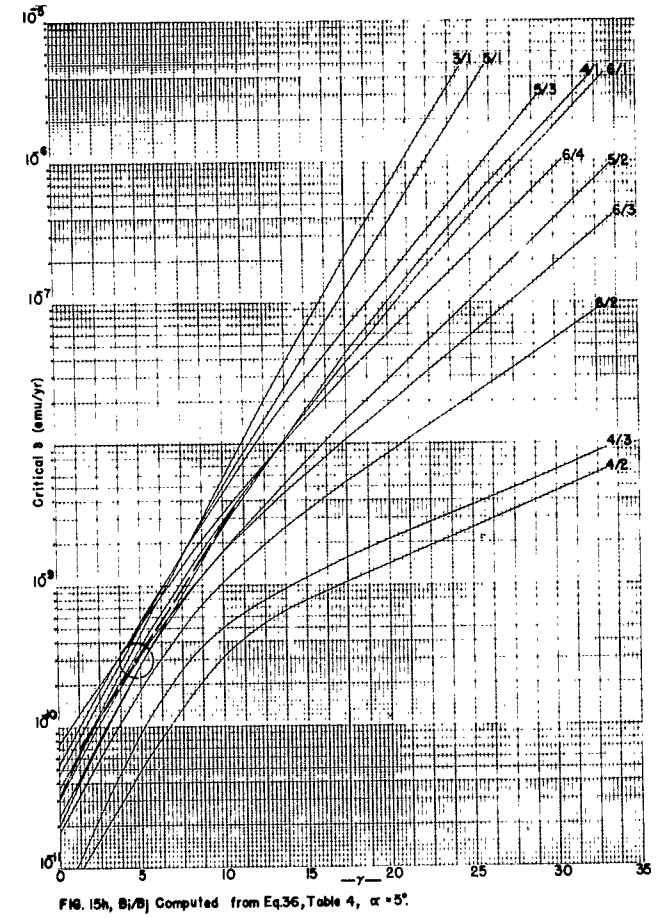

FIG. 15h, B_i/B_j Computed from Eq. 36, Table 4, $\alpha = 5°$.

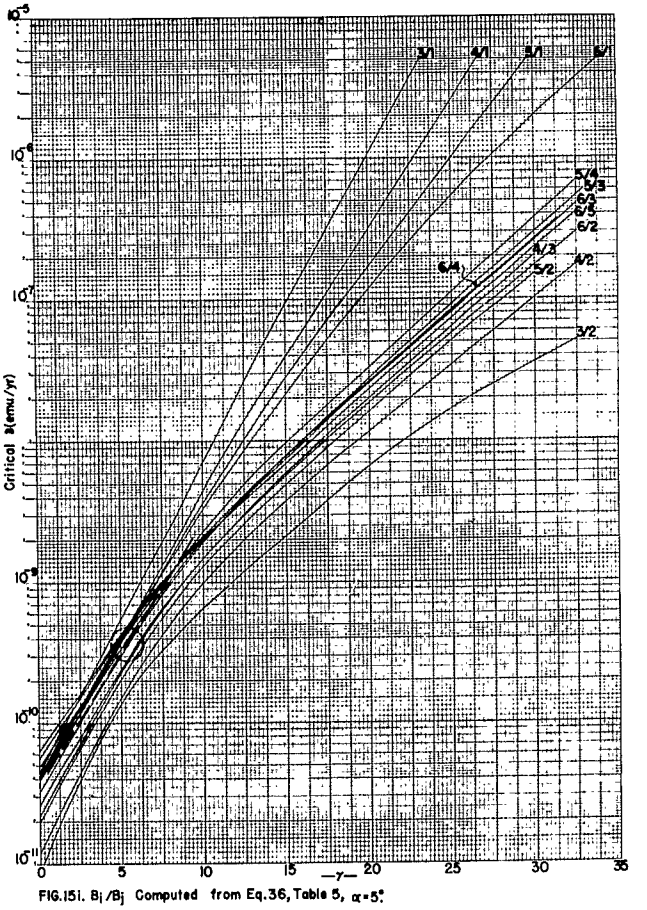

FIG. 15i, B_i/B_j Computed from Eq. 36, Table 5, $\alpha = 5°$.

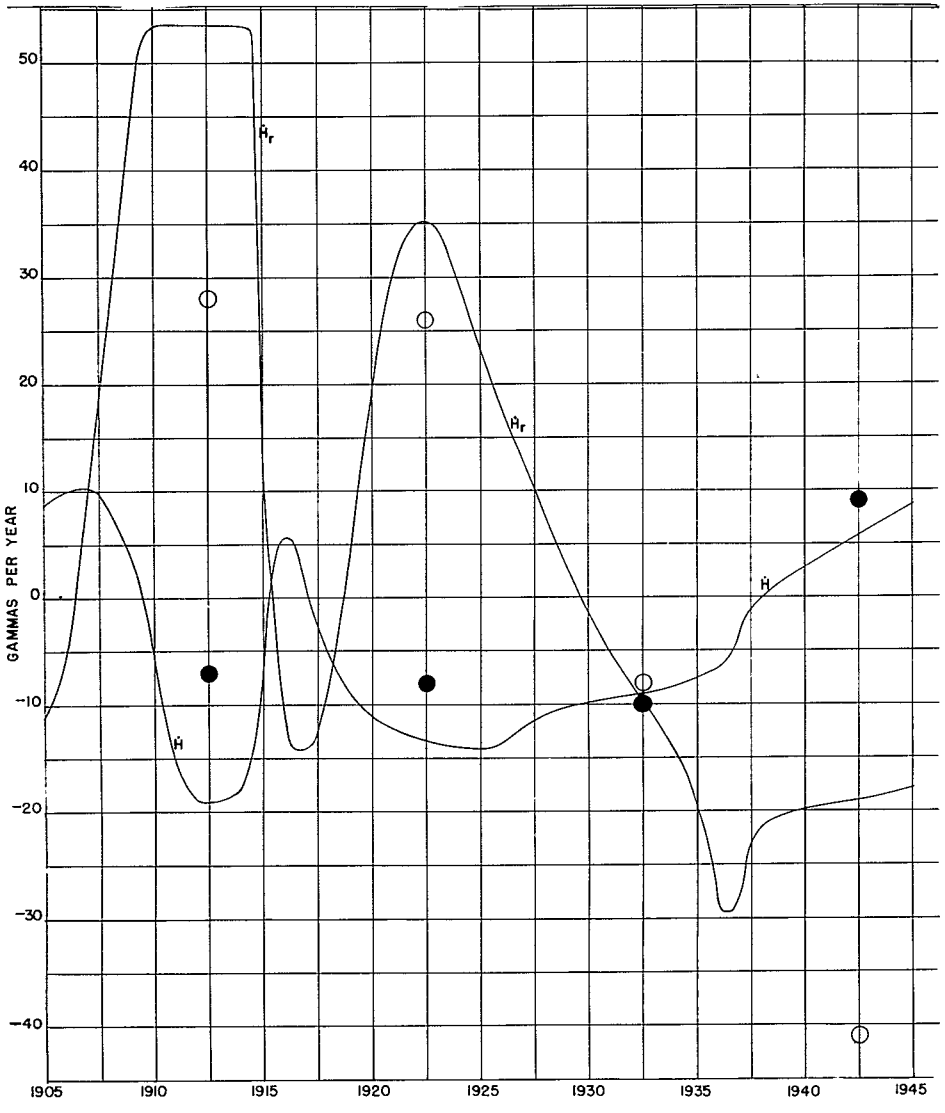

FIG. 16. SECULAR VARIATION at STONYHURST, GREAT BRITAIN

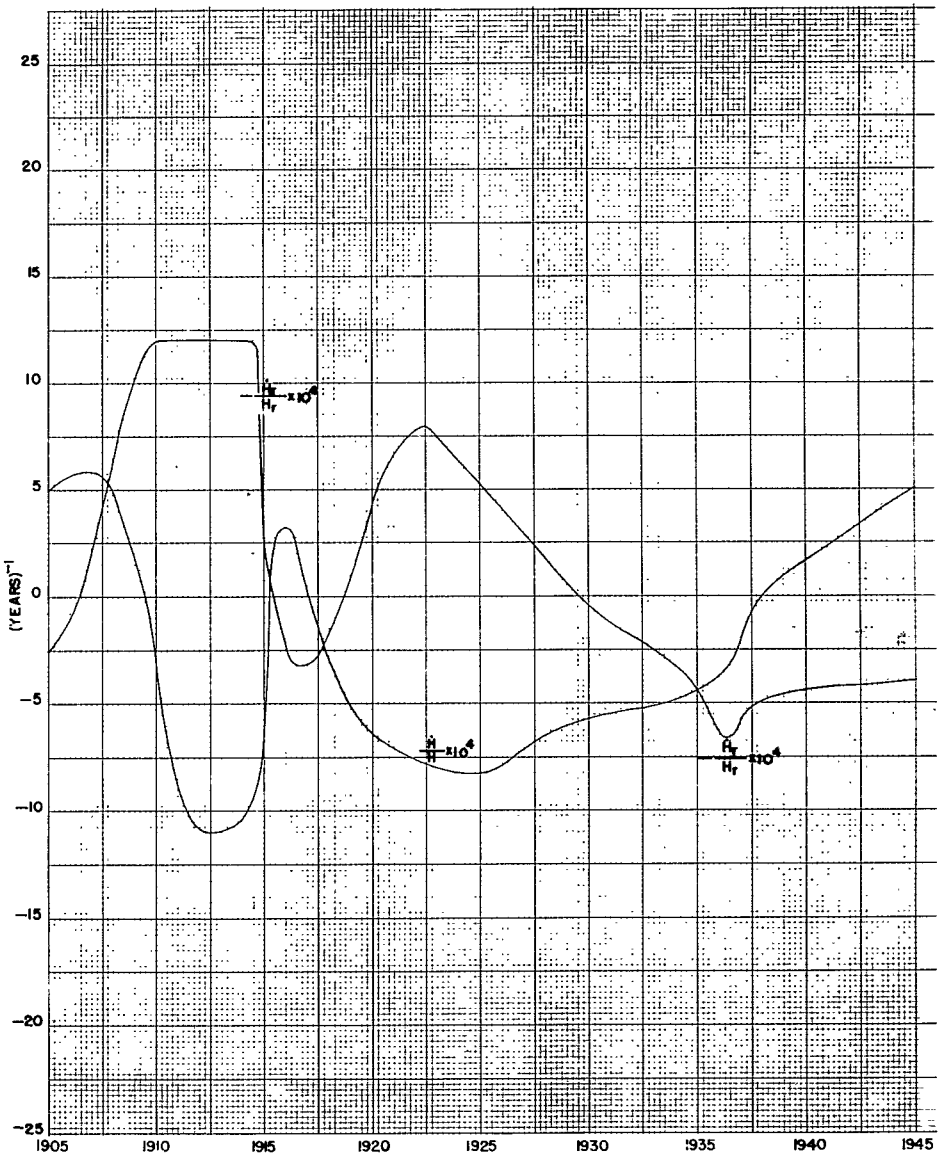

FIG. 17. STONYHURST, GREAT BRITAIN(53.85N357.53E)

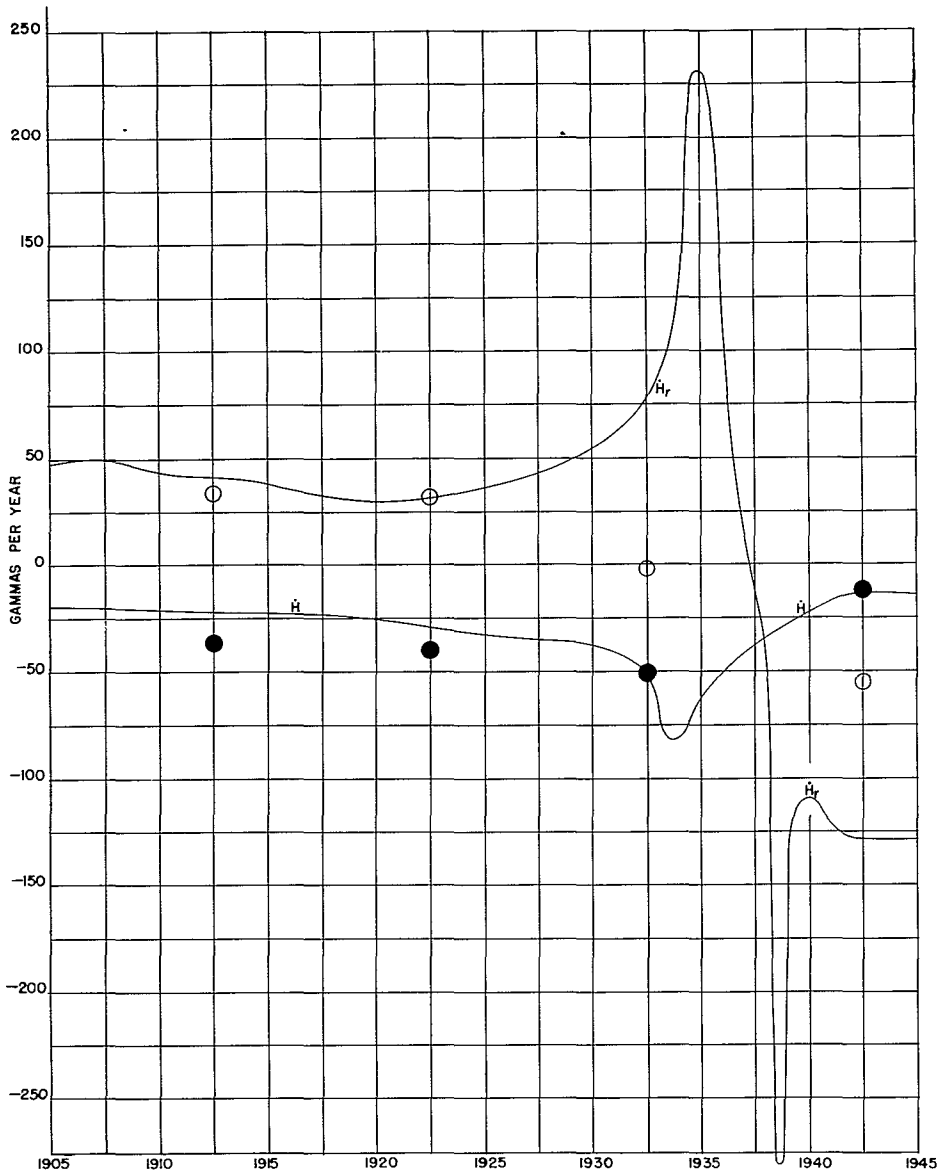

FIG. 18. SECULAR VARIATION at DICKSON, SIBERIA

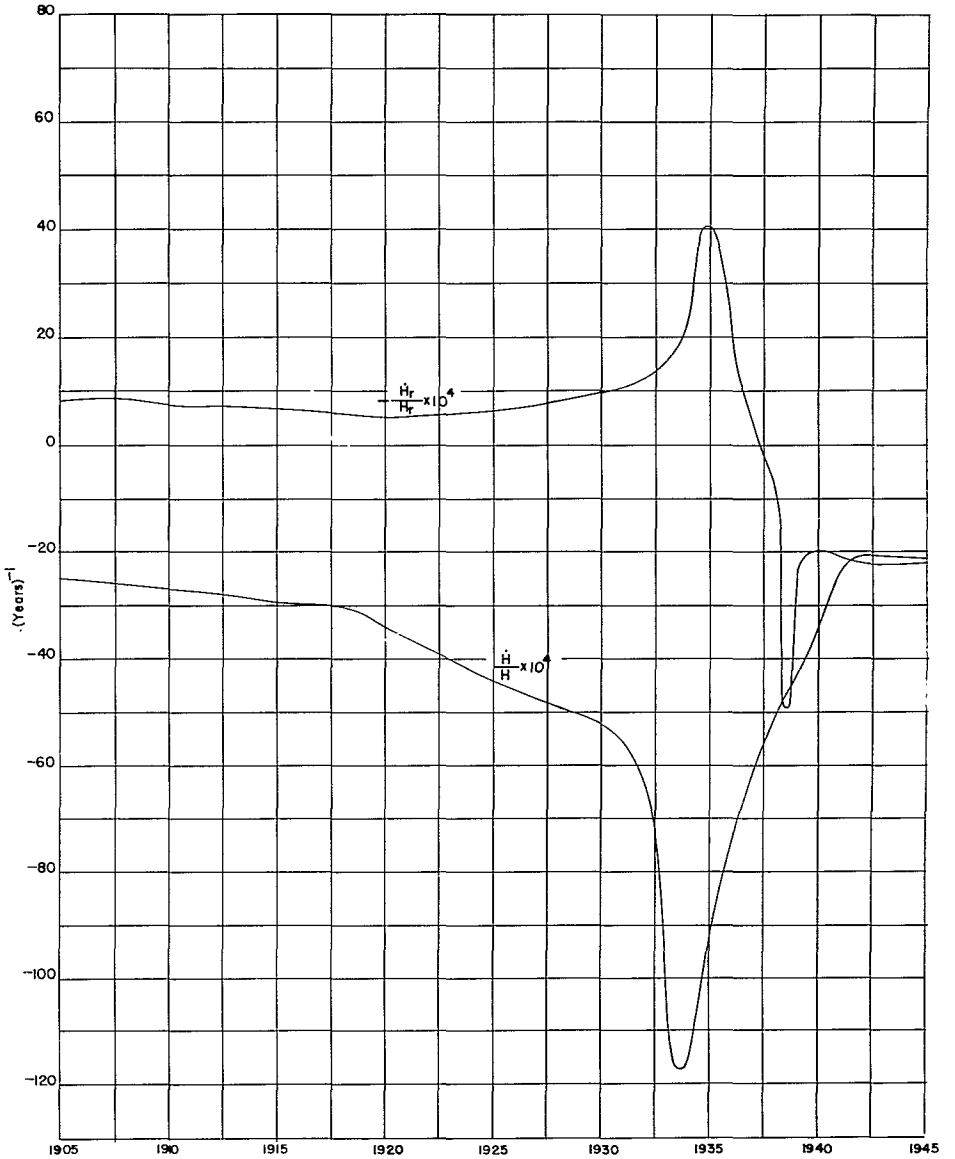

FIG. 19. DICKSON, SIBERIA (73.5N 80.4E)

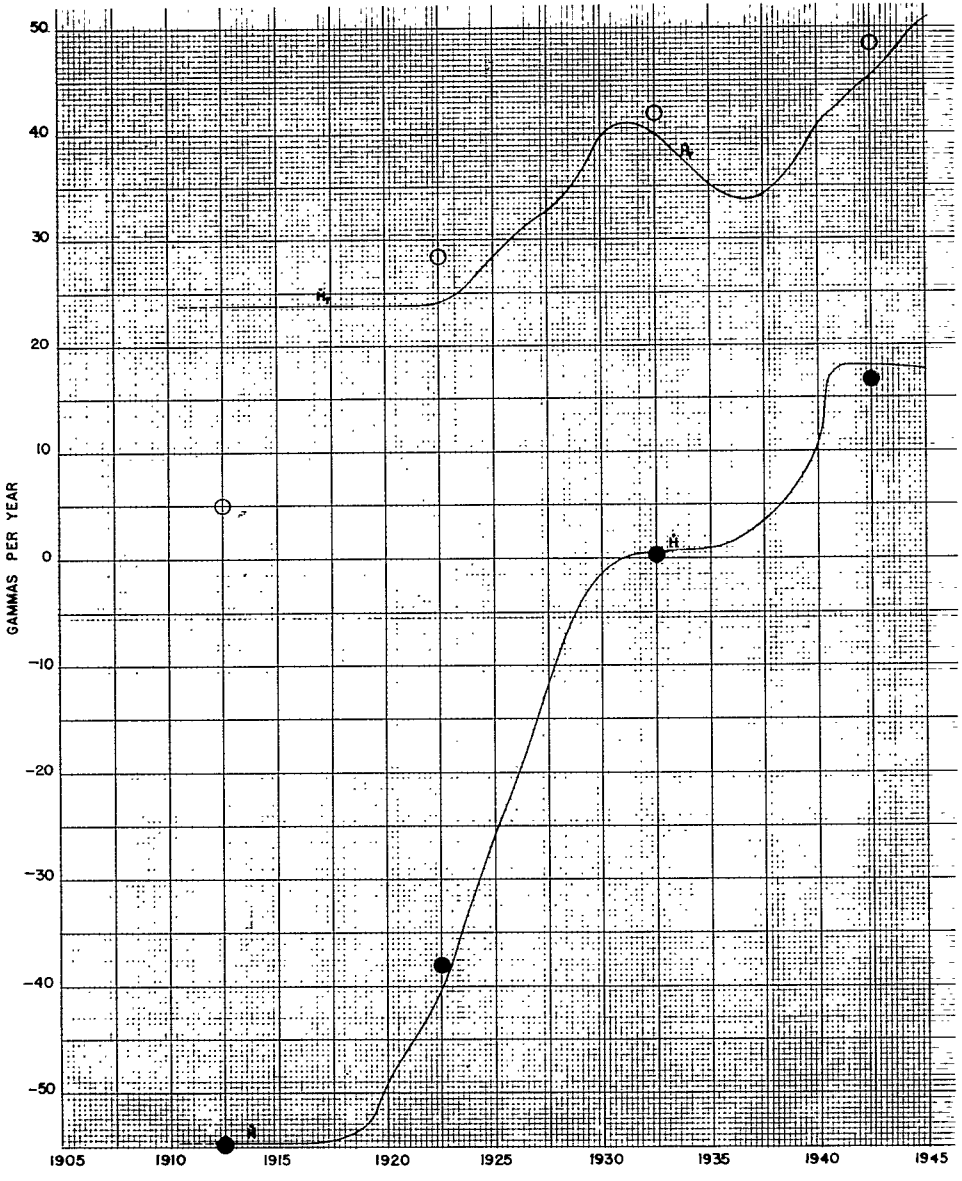

FIG. 20. SECULAR VARIATION at WATHEROO, AUSTRALIA

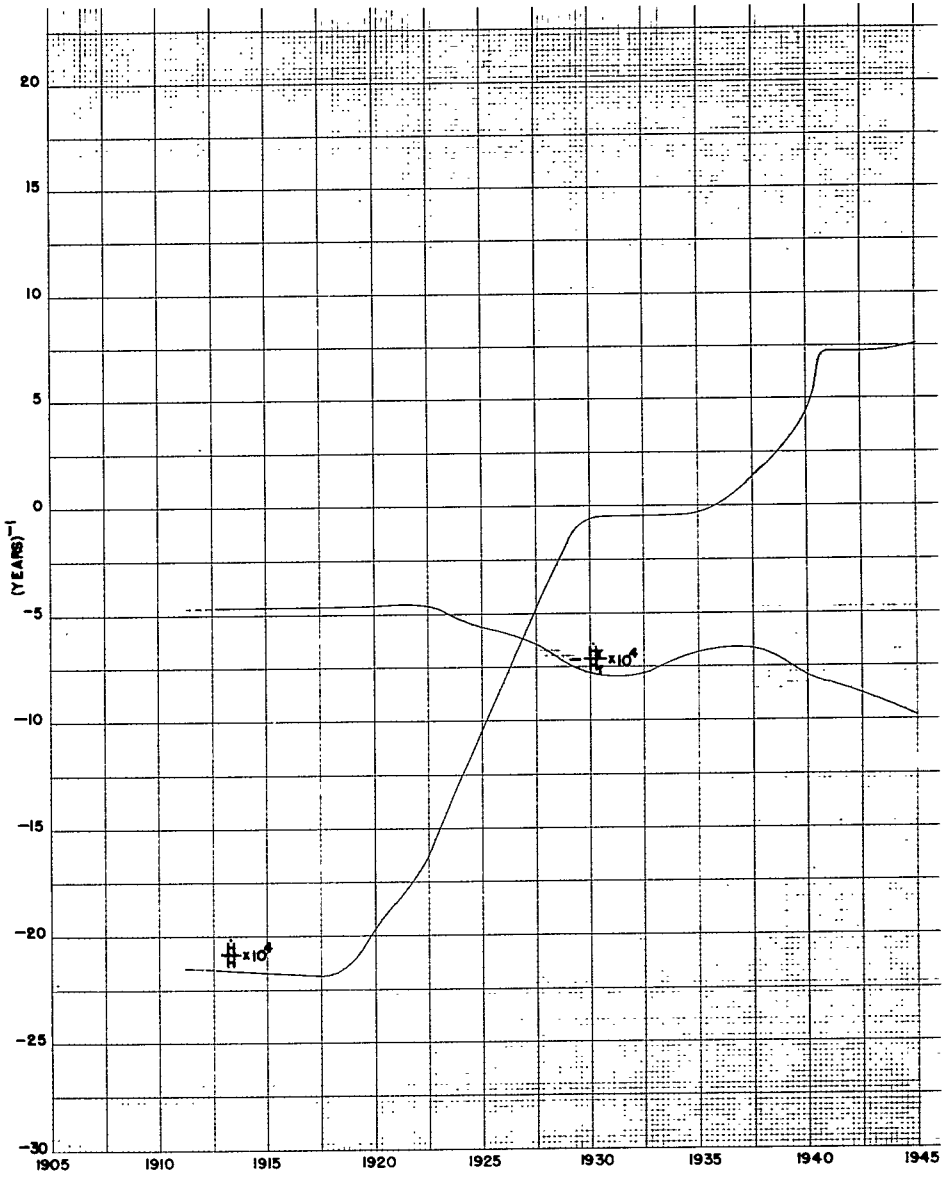

FIG. 21. WATHEROO, AUSTRALIA(30.32S,115.87E)

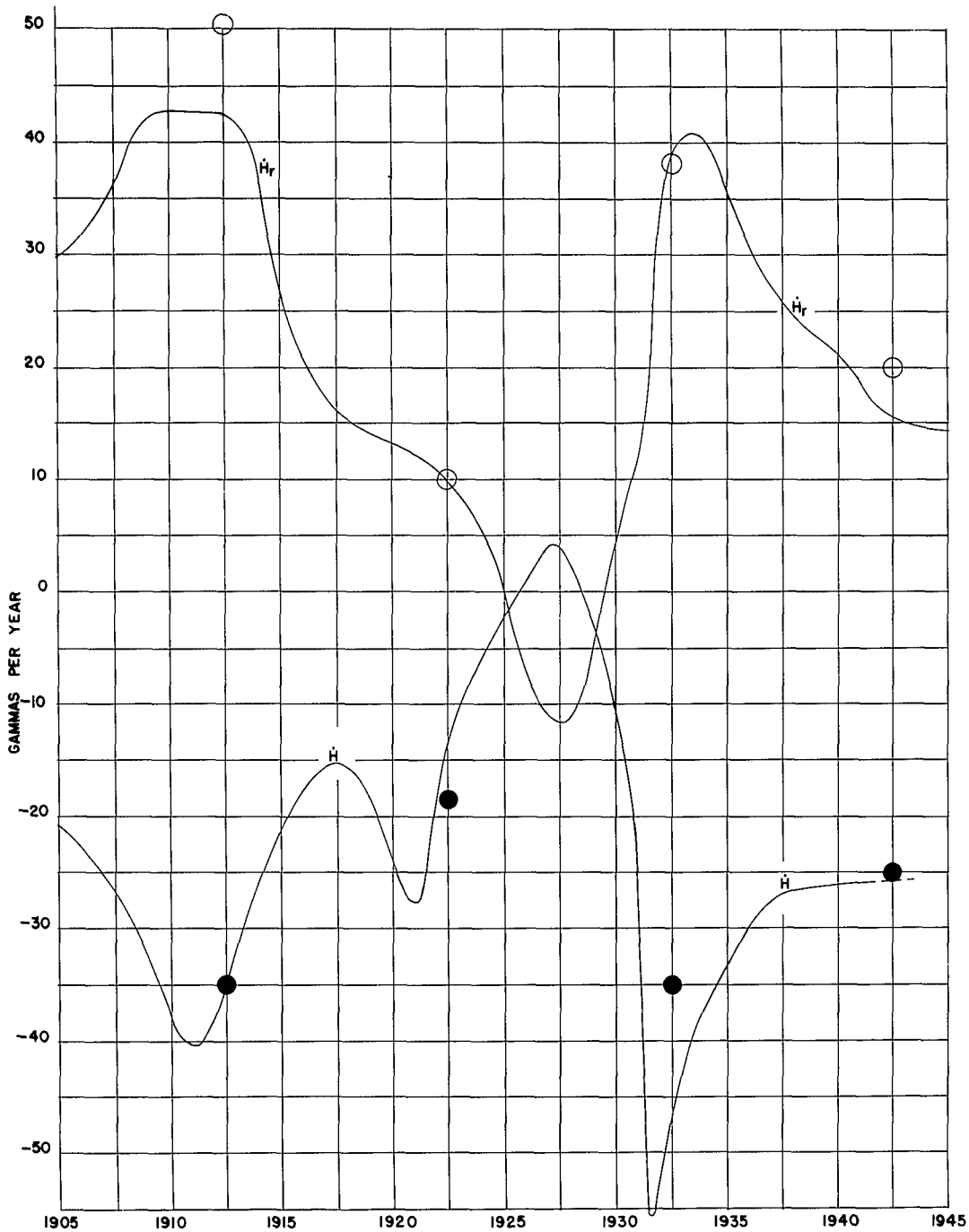

FIG. 22. SECULAR VARIATION at APIA (SOMOA)(13.80S, 188.23E)

DISTRIBUTION LIST

Addressee	No. of Copies
U. S. Navy Hydrographic Office, Washington 25, D. C.	1
Director, Woods Hole Oceanographic Institution, Woods Hole, Massachusetts	1
Director, Scripps Institution of Oceanography, La Jolla, California	1
Director, Lamont Geological Observatory Torrey Cliff, Palisades, New York	1
Director, U. S. Geological Survey, Department of Interior, Washington 25, D. C.	1
U. S. Geological Survey, Geophysics Branch, Washington 25, D. C.	1
Director, Institute of Geophysics, University of California, Los Angeles, California	1
Princeton University, Department of Geology, Princeton, New Jersey	1
Carnegie Institution of Washington, Department of Terrestial Magnetism, Washington 25, D. C.	1
Dr. G. P. Wollard, University of Wisconsin, Madison, Wisconsin	1
Geophysics Branch, Code 416, Office of Naval Research, Washington 25, D. C.	2
Director, Naval Research Laboratory, Attention: Technical Information Officer, Washington 25, D. C.	6
Officer-In-Charge, Office of Naval Research London Branch Office Navy No. 100, Fleet Post Office, New York, New York	2
Office of Naval Research Branch Office, 346 Broadway, New York 13, New York	1
Office of Naval Research Branch Office, Tenth Floor, The John Crerar Library Building, 86 East Randolph Street, Chicago, Illinois	1
Office of Naval Research Branch Office, 1030 East Green Street, Pasadena 1, California	1
Office of Naval Research Branch Office, 1000 Geary Street, San Francisco, California	1
Office of Technical Services, Department of Commerce, Washington 25, D. C.	1
Armed Services Technical Information Center, Documents Service Center, Knott Building, Dayton 2, Ohio	5
Assistant Secretary of Defense for Research and Development, Attention: Committee on Geophysics and Geography, Pentagon Building, Washington 25, D. C.	1